

## Kinematics of shot-geophone migration

Christiaan C. Stolk<sup>1</sup>, Maarten V. de Hoop<sup>2</sup>, and William W. Symes<sup>3</sup>

### ABSTRACT

Recent analysis and synthetic examples have shown that many prestack depth migration methods produce nonflat image gathers containing spurious events, even when provided with a kinematically correct migration velocity field, if this velocity field is highly refractive. This pathology occurs in all migration methods that produce partial images as independent migrations of data bins. Shot-geophone prestack depth migration is an exception to this pattern: each point in the prestack image volume depends explicitly on all traces within the migration aperture. Using a ray-theoretical analysis, we have found that shot-geophone migration produces focused (subsurface-offset domain) or flat (scattering-angle domain) image gathers, provided there is a curvilinear coordinate system defining pseudodepth with respect to which the rays carrying significant energy do not turn, and that the acquisition coverage is sufficient to determine all such rays. Although the analysis is theoretical and idealized, a synthetic example suggests that its implications remain valid for practical implementations, and that shot-geophone prestack depth migration could be a particularly appropriate tool for velocity analysis in a complex structure.

### INTRODUCTION

The basis of migration velocity analysis is the semblance principle: prestack migrated data volumes contain flat image gathers, i.e., are at least kinematically independent of the bin or stacking parameter, when the velocity is correct (Kleyn, 1983; Yilmaz, 1987). Migration velocity analysis (as opposed to standard NMO-based velocity analysis) is needed most urgently in areas of strong lateral velocity variation, i.e., complex structures such as salt flanks, chalk tectonics, and overthrust geology. However, strong refraction implies multiple

raypaths connecting source and receiver locations with reflection points, and multiple raypaths imply that the semblance principle is not valid; i.e., image gathers are not in general flat, even when the migration velocity closely approximates the true propagation velocity (Stolk and Symes, 2004).

The failure of the semblance principle in complex structures afflicts all prestack migration techniques in which each data bin creates an independent (partial) image of the subsurface. This category includes many variants of common-shot, common-offset, and common-scattering-angle migration (Nolan and Symes, 1996, 1997; Xu et al., 2001; Stolk, 2002; Brandsberg-Dahl et al., 2003; Stolk and Symes, 2004). Note that gathers fail to be flat for numerous reasons other than the explanation given in Stolk and Symes (2004). The causes include finite migration aperture and data frequency content, numerical inaccuracies in traveltimes computation or wavefield extrapolation, and (of course) inaccurate migration velocity. The result in Stolk and Symes (2004) shows that, even if all of these other sources of error are corrected, a geometric obstruction to flat gathers remains.

Because these kinematic artifacts interfere destructively (“stack out”) in the final image formation, their presence is mostly an issue for velocity analysis (and possibly for inference of elastic parameters). As shown, for example, in Nolan and Symes (1997), in image gathers produced with inaccurate velocities, the artifacts are indistinguishable from the actual events and thus can obstruct successful velocity updating. The artifacts we are concerned with here are singular artifacts and need to be distinguished from so-called low-frequency artifacts that, for example, have been observed in images obtained with reverse time migration.

However, one well-known form of prestack image formation does not form partial images as independent prestack migrations of data bins: this is Claerbout’s survey-sinking migration (Claerbout, 1971, 1985). This migration method commonly is implemented using an approximate one-way wave equation to extrapolate the source and receiver wavefields. Such depth-extrapolation implementation presumes that rays carrying significant energy do not turn horizontal.

Manuscript received by the Editor 22 January 2009; revised manuscript received 18 June 2009; published online 15 December 2009.

<sup>1</sup>Korteweg-de Vries Institute for Mathematics, Amsterdam, The Netherlands. E-mail: c.c.stolk@uva.nl.

<sup>2</sup>Purdue University, Center for Computational and Applied Mathematics and Geo-Mathematical Imaging Group, West Lafayette, Indiana, U.S.A. E-mail: mdehoop@purdue.edu.

<sup>3</sup>Rice University, Department of Computational and Applied Mathematics, The Rice Inversion Project, Houston, Texas, U.S.A. E-mail: symes@caam.rice.edu.

© 2009 Society of Exploration Geophysicists. All rights reserved.

Source and receiver wavefields might be extrapolated separately and correlated at each depth (shot-profile or shot-record migration), or extrapolated simultaneously (double-square-root [DSR] equation-based migration); in principle, the two produce equivalent image volumes (Stolk and De Hoop, 2001; Biondi, 2003; Stolk and De Hoop, 2005, 2006). In either case, the prestack migration output at each image point depends on a range of sources and receivers, not on data from a single bin defined by fixing any combination of acquisition parameters.

This study comprises an analysis of the kinematics of an idealized version of Claerbout's migration method. We call this, for want of a better name, shot-geophone migration. We emphasize that this term, as used in this study, does not imply any particular method of wavefield extrapolation, or a choice between separate or simultaneous extrapolation of source and receiver wavefields. Our idealized shot-geophone migration encompasses shot-profile and DSR migration methods; all practical realizations of these can be viewed as approximations of our idealized method. In fact, even depth extrapolation (one-way wave propagation) is not intrinsic to the definition of this idealized migration operator. Both two-way reverse time and Kirchhoff (diffraction sum) realizations are possible and inherit the same theoretical properties.

Our analysis demonstrates that a semblance principle appropriate for shot-geophone migration holds (at least theoretically) regardless of velocity field complexity, assuming (1) the single scattering approximation accurately describes the data; (2) there is a curvilinear coordinate system defining pseudodepth with respect to which the rays carrying significant energy do not turn; (3) the survey contains enough data to determine wavefield kinematics (for example, areal or "true 3D" acquisition in general, or narrow-azimuth data plus mild crossline heterogeneity); and (4) the migration velocity field is kinematically correct. In the flat coordinate system, this result was established by Stolk and De Hoop (2001). Here, we give a simpler derivation of this property and extend it to allow for a large class of "turning rays."

The semblance principle appropriate for shot-geophone migration takes several roughly equivalent forms, corresponding to several available methods for forming image gathers. Schultz and Sherwood (1982), Claerbout (1985), and others define image gathers depending on (subsurface) offset and depth; in such offset image gathers, energy is focused at zero offset when the velocity is kinematically correct. De Bruin et al. (1990) and Prucha et al. (1999) give one definition of angle image gathers, and Sava and Fomel (2003) suggest another. Such gathers are functions of scattering angle and depth. In both cases, the correct migration velocity focuses energy at zero slope; i.e., angle image gathers are flattened at the correct migration velocity. In consequence, angle imaging via shot-geophone migration, using either method of angle gather formation mentioned above, is not equivalent, even kinematically, to Kirchhoff common-angle imaging (Xu et al., 2001; Brandsberg-Dahl et al., 2003). Indeed, the latter typically generates kinematic artifacts when multiple raypaths carry important energy.

Theoretical properties are interesting only insofar as they have an observable practical effect. We present a synthetic example in which the prestack image volume has the properties predicted by the theory. We chose an example for which prior analysis already had shown the existence of kinematic artifacts in common-offset or common-scattering-angle Kirchhoff migration. We used a shot-geophone migration based on solving Helmholtz equations (Sirgue and Pratt, 2004). Apart from any implementation defects or limitations of the

data, image amplitudes might have only an indirect relation to reflection strength and might disappear altogether in shadow zones. However, where image energy is present, it will be focused (offset image gathers) or appear in flat events (angle image gathers), with no apparent kinematic artifacts. The apparent fidelity of the examples to the theory also supports our contention that the theoretical predictions of our analysis survive implementation imperfections.

The semblance principle is a result of the mathematical structure of shot-geophone migration, not of any particular approach to its implementation. Migration operators are dual or the adjoint to modeling operators. The various prestack migration operators are the adjoint to extended Born modeling operators, and differ in the way in which Born modeling is extended. The ray geometry of these extended modeling operators is central to our analysis. The semblance principle and imaging condition of each prestack migration operator are inherent in the definition of the corresponding extended Born model, which in some sense explains these concepts.

Schultz and Sherwood (1982) observe that the focusing property of shot-geophone migration might serve as the basis for an approach to velocity estimation. Velocity analysis based on focusing is considered also by Faye and Jeannot (1986), MacKay and Abma (1992), and Nemeth (1995). Its freedom from artifacts suggests that shot-geophone migration could be a particularly appropriate tool for migration velocity analysis of data acquired over complex structures. Some investigations of this idea have been carried out (Shen et al., 2003; Sava and Biondi, 2004; Albertin et al., 2006; De Hoop et al., 2006).

We begin with a description of the idealized shot-geophone migration operator as the adjoint to an extended Born (single-scattering) modeling operator. All prestack migration methods, including those based on data binning, can be described in this way: as the adjoint to extended modeling of some sort. The basic kinematics of shot-geophone prestack migration then follow easily from the high-frequency asymptotics of wave propagation. We summarize these kinematic properties and present the outline of a complete derivation in Appendix A. The artifact-free result of Stolk and De Hoop (2001) follows readily from the general kinematic properties already described, for offset image gathers and angle image gathers in the style of Sava and Fomel (2003).

We also review an alternative construction of angle image gathers because of De Bruin et al. (1990). We show how the semblance property for this form of angle-domain migration, extended to curvilinear coordinates, follows from the general properties of shot-geophone migration in Appendix B. Finally, we present an example illustrating the semblance property, using 2D synthetic data of significant ray-path complexity. The example contrasts the angle image gathers produced by (Kirchhoff or generalized Radon transform) common-scattering-angle migration (De Hoop and Bleistein, 1997; Xu et al., 2001; Brandsberg-Dahl et al., 2003) with those produced by shot-geophone migration. Kinematic artifacts appear and can be unambiguously identified as kinematic artifacts in the former, but do not appear in the latter. See Table 1 for our notation of fields and operators.

## SHOT-GEOPHONE MIGRATION AS THE ADJOINT OF EXTENDED BORN MODELING

We assume that sources and receivers lie on the same depth plane, and we adjust the depth axis so that the source-receiver plane is  $z = 0$ . This restriction can be removed at the cost of more complicated

notation (and numerics): it is not essential. Nothing about the formulation of the migration method presented below requires that data be given on the full surface  $z = 0$ .

Although all of the examples to be presented later are two-dimensional, the construction is not. In the following,  $\mathbf{x}$  (and other boldface letters) denote either two- or three-dimensional vectors. Source locations are  $\mathbf{x}_s$ ; receiver locations are  $\mathbf{x}_r$ .

### Single scattering

The causal acoustic Green's function  $G(\mathbf{x}, t; \mathbf{x}_s)$  for a point source at  $\mathbf{x} = \mathbf{x}_s$  is the solution of

$$\frac{1}{v^2(\mathbf{x})} \frac{\partial^2 G}{\partial t^2}(\mathbf{x}, t; \mathbf{x}_s) - \nabla_{\mathbf{x}}^2 G(\mathbf{x}, t; \mathbf{x}_s) = \delta(\mathbf{x} - \mathbf{x}_s) \delta(t), \quad (1)$$

with  $G = 0, t < 0$ .

In common with all other migration methods, shot-geophone migration is based on the Born or single-scattering approximation. Denote by  $r(\mathbf{x}) = \delta v(\mathbf{x})/v(\mathbf{x})$  a relative perturbation of the velocity field. Linearization of the wave equation yields for the corresponding perturbation of the Green's function

$$\frac{1}{v^2(\mathbf{x})} \frac{\partial^2 \delta G}{\partial t^2}(\mathbf{x}, t; \mathbf{x}_s) - \nabla_{\mathbf{x}}^2 \delta G(\mathbf{x}, t; \mathbf{x}_s) = \frac{2r(\mathbf{x})}{v^2(\mathbf{x})} \frac{\partial^2}{\partial t^2} G(\mathbf{x}, t; \mathbf{x}_s), \quad (2)$$

whose solution has the integral representation at the source and receiver points  $\mathbf{x}_r, \mathbf{x}_s$ ,

$$\delta G(\mathbf{x}_r, t; \mathbf{x}_s) = \frac{\partial^2}{\partial t^2} \int d\mathbf{x} \frac{2r(\mathbf{x})}{v^2(\mathbf{x})} \int d\tau G(\mathbf{x}, t - \tau; \mathbf{x}_r) G(\mathbf{x}, \tau; \mathbf{x}_s). \quad (3)$$

In equation 2, we assume that the background velocity field  $v$  is smooth, whereas the perturbation  $r$  captures the discontinuities.

The singly scattered field is the time convolution of  $\delta G$  with a source wavelet (or the space-time convolution with a radiation pattern operator, for more complex sources). Because the principal concern of this study involves kinematic relationships between the data and image, we ignore the filtering by the source signature (i.e., replace it with a delta function). This effective replacement of the source by an impulse does not seem to invalidate the predictions of the theory, although the matter is certainly worthy of more study.

The Born modeling operator  $F[v]$  is

$$F[v]r(\mathbf{x}_r, t; \mathbf{x}_s) = \delta G(\mathbf{x}_r, t; \mathbf{x}_s). \quad (4)$$

### Common-offset modeling and migration

Basic versions of all prestack migration operators result from two additional modeling steps: (1) extend the definition of reflectivity to depend on more spatial degrees of freedom, inserted somehow into the Born modeling formula (equation 2 or 3) in such a way that when the extra degrees of freedom are present in some specific way ("physical reflectivity"), Born modeling is recovered, and (2) form the adjoint of the extended modeling operator: this is a prestack migration operator. The output of the adjoint operator is the prestack image; it depends on the same degrees of freedom as the input of the modeling operator.

Prestack common-offset modeling results from replacing  $2r(\mathbf{x})/v^2(\mathbf{x})$  with  $R(\mathbf{x}, \mathbf{h})$ , where  $\mathbf{h}$  is vector half-offset:  $\mathbf{h} = \frac{1}{2}(\mathbf{x}_r - \mathbf{x}_s)$ ;  $\mathbf{x}$  is not necessarily located below the midpoint. Denote by  $\mathbf{x}_m = \frac{1}{2}(\mathbf{x}_r + \mathbf{x}_s)$  the corresponding midpoint vector.

The additional degrees of freedom mentioned in step one above are the components of the source-receiver half-offset. This extended reflectivity is inserted into the Born modeling formula to give the extended common-offset modeling operator  $\bar{F}_{\text{co}}[v]$ :

$$\bar{F}_{\text{co}}[v]R(\mathbf{x}_r, t; \mathbf{x}_s) = u(\mathbf{x}_r, t; \mathbf{x}_s), \quad (5)$$

where

$$u(\mathbf{x}_m + \mathbf{h}, t; \mathbf{x}_m - \mathbf{h}) = \frac{\partial^2}{\partial t^2} \int d\mathbf{x} R(\mathbf{x}, \mathbf{h}) \int d\tau \times G(\mathbf{x}, t - \tau; \mathbf{x}_m + \mathbf{h}) G(\mathbf{x}, \tau; \mathbf{x}_m - \mathbf{h}). \quad (6)$$

If  $R(\mathbf{x}, \mathbf{h}) = 2r(\mathbf{x})/v^2(\mathbf{x})$  is actually independent of  $\mathbf{h}$ , then the output  $u(\mathbf{x}_r, t; \mathbf{x}_s)$  of equation 6 is identical to the perturbational Green's function  $\delta G(\mathbf{x}_r, t; \mathbf{x}_s)$  as is clear from comparing equations 6 and 3. In other words, the Born forward modeling operator is the "spray" operator

$$r(\mathbf{x}) \mapsto R(\mathbf{x}, \mathbf{h}) = 2r(\mathbf{x})/v^2(\mathbf{x}), \quad (7)$$

followed by the extended common-offset modeling operator.

**Table 1. List of fields and operators.**

Symbol	Description	Equation
$d$	Reflection data	8
$v$	Velocity field	2
$r$	Reflectivity	2
$\tilde{g}$	Riemannian metric	37
$S$	Action functional	39
$G$	Green's function	1
$\delta G$	Single-scattered field	3
$F$	Born modeling operator	4
$R, \bar{R}$	Extended reflectivity	6 and 16
$\bar{F}_{\text{co}}$	Common-offset modeling operator	5 and 6
$\bar{F}$	Shot-geophone modeling operator	9 and 10
$\bar{F}_z$	Restricted modeling operator	25 and 26
$w_s$	Source field	18
$u^*$	Adjoint field	19
$D, \bar{D}$	Sunken survey	32
$I_{\text{co}}$	Common-offset imaging	8
$I_{s-g}, \bar{I}_{s-g}$	Shot-geophone imaging	13 and 17
$I_{s-g,z}$	"Horizontal" subsurface offset imaging	30
$A_z$	Generation of image gathers via Radon transform in offset, depth	31
$B_z$	Generation of image gathers via Radon transform in offset, time	34

The common-offset migration operator is the adjoint of this integral operator; its output is the offset-dependent prestack image volume, a function of the same type as the extended common-offset reflectivity:

$$\begin{aligned} \bar{F}_{\text{co}}^*[v]d(\mathbf{x}, \mathbf{h}) &= I_{\text{co}}(\mathbf{x}, \mathbf{h}), \\ I_{\text{co}}(\mathbf{x}, \mathbf{h}) &= \int d\mathbf{x}_m \int dt \frac{\partial^2 d}{\partial t^2}(\mathbf{x}_m + \mathbf{h}, t; \mathbf{x}_m - \mathbf{h}) \\ &\quad \times \int d\tau G(\mathbf{x}, t - \tau; \mathbf{x}_m + \mathbf{h}) G(\mathbf{x}, \tau; \mathbf{x}_m - \mathbf{h}). \end{aligned} \quad (8)$$

Therefore, the adjoint of Born modeling (migration, per se) is common-offset migration followed by the adjoint of the “spray” operator: this adjoint is the operator that sums or integrates in  $\mathbf{h}$ , i.e., the stack operator.

Actually, the operator defined in equation 8 is only one possible common-offset migration operator. Many others follow through the application of various weights, filters, and approximations. For example, leaving off the second time derivative in equation 8 amounts to filtering the data before the application of  $\bar{F}_{\text{co}}^*[v]$ . Most notably, replacement of the Green’s functions in equation 8 by the leading terms in their high-frequency asymptotic expansions results in the familiar Kirchhoff common-offset migration operator. All of these variations define adjoints to (approximations of) the modeling operator with respect to appropriate inner products on domain and range spaces. Most important for this investigation, all share a common kinematic description. Therefore we ignore all such variations for the time being, and refer to equation 8 as defining “the” common-offset migration operator.

Note that both modeling and migration operators share the property that their output for a given  $\mathbf{h}$  depends only on the input for the same value of  $\mathbf{h}$ ; i.e., they are block diagonal on common-offset data bins. This binwise action is responsible for the production of kinematic artifacts when the velocity field refracts rays sufficiently strongly (Stolk and Symes, 2004).

### Shot-geophone modeling and migration

Shot-geophone modeling results from a different extension of reflectivity: replace  $2r(\mathbf{x})/v^2(\mathbf{x})$  by  $R(\mathbf{x}, \mathbf{h})$ , where  $\mathbf{h}$  is the subsurface (half)-offset mentioned in the introduction. Although this extension has exactly the same degrees of freedom as the common-offset extended reflectivity, the two are conceptually quite different;  $\mathbf{h}$  here has nothing to do with the surface source-receiver half-offset  $\frac{1}{2}(\mathbf{x} - \mathbf{x}_s)$ .

The shot-geophone modeling operator  $\bar{F}[v]$  is given by

$$\bar{F}[v]R(\mathbf{x}_r, t; \mathbf{x}_s) = u(\mathbf{x}_r, t; \mathbf{x}_s), \quad (9)$$

where the field  $u$  is defined by

$$\begin{aligned} u(\mathbf{x}_r, t; \mathbf{x}_s) &= \frac{\partial^2}{\partial t^2} \int d\mathbf{x} \int d\mathbf{h} R(\mathbf{x}, \mathbf{h}) \\ &\quad \times \int d\tau G(\mathbf{x} + \mathbf{h}, t - \tau; \mathbf{x}_r) G(\mathbf{x} - \mathbf{h}, \tau; \mathbf{x}_s). \end{aligned} \quad (10)$$

Note that here,  $\mathbf{x}$  does play the role of subsurface midpoint, although

having nothing to do with the surface source-receiver midpoint.

The field  $u(\mathbf{x}, t; \mathbf{x}_s)$  is identical to  $\delta G(\mathbf{x}, t; \mathbf{x}_s)$  when

$$R(\mathbf{x}, \mathbf{h}) = \frac{2r(\mathbf{x})}{v^2(\mathbf{x})} \delta(\mathbf{h}), \quad (11)$$

i.e., when the generalized reflectivity is concentrated at offset zero. Therefore Born modeling is shot-geophone modeling following the mapping

$$r(\mathbf{x}) \mapsto \frac{2r(\mathbf{x})}{v^2(\mathbf{x})} \delta(\mathbf{h}). \quad (12)$$

The shot-geophone migration operator is the adjoint of the shot-geophone modeling operator. It produces an image volume with the same degrees of freedom as the extended shot-geophone reflectivity,

$$\begin{aligned} \bar{F}^*[v]d(\mathbf{x}, \mathbf{h}) &= I_{\text{s-g}}(\mathbf{x}, \mathbf{h}), \\ I_{\text{s-g}}(\mathbf{x}, \mathbf{h}) &= \int d\mathbf{x}_r \int d\mathbf{x}_s \int dt \frac{\partial^2 d}{\partial t^2}(\mathbf{x}_r, t; \mathbf{x}_s) \\ &\quad \times \int d\tau G(\mathbf{x} + \mathbf{h}, t - \tau; \mathbf{x}_r) G(\mathbf{x} - \mathbf{h}, \tau; \mathbf{x}_s). \end{aligned} \quad (13)$$

Note that in equations 10 and 13 all input variables are integrated to produce the value at each output vector. The computation is not block diagonal in  $\mathbf{h}$ , in contrast to the common-offset operators defined in equations 6 and 8.

Born migration is shot-geophone migration followed by the adjoint of the mapping defined in equation 12, which is

$$R(\mathbf{x}, \mathbf{h}) \mapsto \frac{2R(\mathbf{x}, 0)}{v^2(\mathbf{x})}, \quad (14)$$

or shot-geophone migration followed by extraction of the zero-offset section.

For some purposes, it turns out to be convenient to introduce sunken source and receiver coordinates

$$\bar{\mathbf{x}}_r = \mathbf{x} + \mathbf{h}, \quad \bar{\mathbf{x}}_s = \mathbf{x} - \mathbf{h}, \quad (15)$$

and the source-receiver reflectivity  $\bar{R}$  by

$$\begin{aligned} \bar{R}(\bar{\mathbf{x}}_r, \bar{\mathbf{x}}_s) &= R\left(\frac{\bar{\mathbf{x}}_r + \bar{\mathbf{x}}_s}{2}, \frac{\bar{\mathbf{x}}_r - \bar{\mathbf{x}}_s}{2}\right), \text{ i.e., } \bar{R}(\mathbf{x} + \mathbf{h}, \mathbf{x} - \mathbf{h}) \\ &= R(\mathbf{x}, \mathbf{h}), \end{aligned} \quad (16)$$

and similarly for the image volume  $I_{\text{s-g}}$ . Change the integration variables in equation 13 to get the sunken source-receiver variant of shot-geophone migration:

$$\begin{aligned} \bar{I}_{\text{s-g}}(\bar{\mathbf{x}}_r, \bar{\mathbf{x}}_s) &= \int d\mathbf{x}_r \int d\mathbf{x}_s \int dt \frac{\partial^2 d}{\partial t^2}(\mathbf{x}_r, t; \mathbf{x}_s) \\ &\quad \times \int d\tau G(\bar{\mathbf{x}}_r, t - \tau; \mathbf{x}_r) G(\bar{\mathbf{x}}_s, \tau; \mathbf{x}_s). \end{aligned} \quad (17)$$

Replacement of the Green’s functions in this formula by their high-frequency asymptotic (ray-theoretical) approximations results in a Kirchhoff-like representation of shot-geophone migration.

### Adjoint state formulation

Equation 17 can be reproduced by solving (forward in time) the wave equation for the source field  $w_s$ ,

$$\frac{1}{v^2(\mathbf{x})} \frac{\partial^2 w_s}{\partial t^2}(\mathbf{x}, t; \mathbf{x}_s) - \nabla_{\mathbf{x}}^2 w_s(\mathbf{x}, t; \mathbf{x}_s) = \delta(t) \delta(\mathbf{x} - \mathbf{x}_s), \quad (18)$$

in parallel with solving (backward in time) the wave equation for the adjoint field  $u^*$ ,

$$\begin{aligned} \frac{1}{v^2(\mathbf{x})} \frac{\partial^2 u^*}{\partial t^2}(\mathbf{x}, t; \mathbf{x}_s) - \nabla_{\mathbf{x}}^2 u^*(\mathbf{x}, t; \mathbf{x}_s) \\ = \int d\mathbf{x}' \frac{\partial^2 d}{\partial t^2}(\mathbf{x}', t; \mathbf{x}_s) \delta(\mathbf{x} - \mathbf{x}'), \end{aligned} \quad (19)$$

followed by the crosscorrelation at zero time lag,

$$\bar{I}_{s-g}(\bar{\mathbf{x}}_r, \bar{\mathbf{x}}_s) = \int d\mathbf{x}_s \int d\tau u^*(\bar{\mathbf{x}}_r, \tau; \mathbf{x}_s) w_s(\bar{\mathbf{x}}_s, \tau; \mathbf{x}_s). \quad (20)$$

(An implementation of this formulation avoids asymptotic approximations inherent in the downward-continuation formulation, and admits, in principle, highly irregular source and receiver spacing as these appear in global earth applications. The construction of one-way wave equations in the presence of general vertical and lateral velocity variation, and making use of techniques from microlocal analysis, used in the downward-continuation formulation, holds only asymptotically.)

### KINEMATICS OF SHOT-GEOPHONE MIGRATION

An event in the data is characterized by its moveout: locally, by a moveout equation  $t = T(\mathbf{x}_r, \mathbf{x}_s)$ , and infinitesimally by the source and receiver slownesses

$$\mathbf{p}_r = \nabla_{\mathbf{x}_r} T, \quad \mathbf{p}_s = \nabla_{\mathbf{x}_s} T. \quad (21)$$

Significant energy with this moveout implies that locally near  $(\mathbf{x}_r, \mathbf{x}_s, t)$  the data contains a plane-wave component with wavenumber  $(\omega \mathbf{p}_r, \omega \mathbf{p}_s, \omega)$ ,  $\omega$  being temporal frequency. These coordinates (position, wavenumber) give the (geometric) phase space representation of the event.

Note that for incomplete coverage (aperture or sampling), an event in the data typically will not determine its moveout uniquely. For example, in conventional marine streamer geometry, with the streamers oriented along the  $x$ -axis, the  $y$ -component of  $\mathbf{p}_r$  is not determined by the data. However, in present-day (possibly zigzag) wide-azimuth towed streamer (WATS) acquisition geometry (Michell et al., 2006; Barley and Summers, 2007),  $\mathbf{p}_r$  and  $\mathbf{p}_s$  are determined. In the discussion to follow,  $\mathbf{p}_s$  and  $\mathbf{p}_r$  are assumed to be compatible with a reflection event. Likewise, a reflector (in the source-receiver representation) at  $(\bar{\mathbf{x}}_r, \bar{\mathbf{x}}_s)$  with wavenumber  $(\mathbf{k}_r, \mathbf{k}_s)$  is characterized in (image volume) phase space by these coordinates.

### Kinematics with general (3D) subsurface offset

The kinematic description of shot-geophone migration relates the phase space coordinates of events and reflectors. An event or reflection with phase space representation

$$(\mathbf{x}_r, \mathbf{x}_s, T(\mathbf{x}_r, \mathbf{x}_s), \omega \mathbf{p}_r, \omega \mathbf{p}_s, \omega) \quad (22)$$

is the result of a reflector with (source-receiver) phase space representation  $(\bar{\mathbf{x}}_r, \bar{\mathbf{x}}_s, \mathbf{k}_r, \mathbf{k}_s)$  exactly when both of the following occur:

- A ray  $(\mathbf{X}_s, \mathbf{P}_s)$  is leaving the source point  $\mathbf{X}_s(0) = \mathbf{x}_s$  at time  $t = 0$  with ray parameter  $\mathbf{P}_s(0) = \mathbf{p}_s$  and arriving at  $\mathbf{X}_s(t_s) = \bar{\mathbf{x}}_s$  at  $t = t_s$  with ray parameter  $\mathbf{P}_s(t_s) = -\mathbf{k}_s / \omega$ .
- A ray  $(\mathbf{X}_r, \mathbf{P}_r)$  is leaving  $\mathbf{X}_r(t_s) = \bar{\mathbf{x}}_r$  at  $t = t_s$  with ray parameter  $\mathbf{P}_r(t_s) = \mathbf{k}_r / \omega$  and arriving at the receiver point  $\mathbf{X}_r(t_r + t_s) = \mathbf{x}_s$  at time  $t = T(\mathbf{x}_r, \mathbf{x}_s) = t_r + t_s$  with ray parameter  $\mathbf{P}_r(t_r + t_s) = \mathbf{p}_r$ .

Figure 1 illustrates this kinematic relation. Appendix A provides a derivation.

Note that because  $\mathbf{P}_r, \mathbf{P}_s$  are ray slowness vectors, a length relation necessarily exists between  $\mathbf{k}_r, \mathbf{k}_s$ , namely,

$$\begin{aligned} \frac{1}{v(\bar{\mathbf{x}}_r)} &= \|\mathbf{P}_r(t_r)\| = \frac{\|\mathbf{k}_r\|}{|\omega|}, \\ \frac{1}{v(\bar{\mathbf{x}}_s)} &= \|\mathbf{P}_s(t_s)\| = \frac{\|\mathbf{k}_s\|}{|\omega|}, \end{aligned} \quad (23)$$

whence

$$\frac{\|\mathbf{k}_r\|}{\|\mathbf{k}_s\|} = \frac{v(\bar{\mathbf{x}}_s)}{v(\bar{\mathbf{x}}_r)}. \quad (24)$$

The kinematics of shot-geophone migration are somewhat strange, so it is reassuring to see that for physical reflectors (i.e.,  $R(\mathbf{x}, \mathbf{h}) = r(\mathbf{x}) \delta(\mathbf{h})$ ) the relation just explained becomes the familiar one of reflection from a reflecting element according to Snell's law. A quick calculation shows that such a physical  $\bar{R}$  (cf. equation 16) has a significant local plane-wave component near  $(\bar{\mathbf{x}}_r, \bar{\mathbf{x}}_s)$  with wavenumber  $(\mathbf{k}_r, \mathbf{k}_s)$  only if  $\bar{\mathbf{x}}_r = \bar{\mathbf{x}}_s = \mathbf{x}$  and  $r$  has a significant local plane-wave component near  $\mathbf{x}$  with wavenumber  $\mathbf{k}_x = \mathbf{k}_r + \mathbf{k}_s$ . From equation 24,  $\mathbf{k}_r$  and  $\mathbf{k}_s$  have the same length; therefore their sum  $\mathbf{k}_x$  is also their bisector, which establishes Snell's law. Thus a single (physical) reflector at  $\mathbf{x}$  with wavenumber  $\mathbf{k}_x$  gives rise to a reflected event at frequency  $\omega$  exactly when the rays  $(\mathbf{X}_s, \mathbf{P}_s)$  and  $(\mathbf{X}_r, \mathbf{P}_r)$  meet at  $\mathbf{x}$  at time  $t_s$ , and the reflector dip  $\mathbf{k}_x = \omega(\mathbf{P}_r(t_s) - \mathbf{P}_s(t_s))$ , which is the usual kinematics of single scattering. See Figure 2.

It is possible now to answer this question: In the shot-geophone model, to what extent does a data event determine the corresponding reflector? The rules derived above show that the reflection point  $(\bar{\mathbf{x}}_s, \bar{\mathbf{x}}_r)$  must lie on the Cartesian product of two rays  $(\mathbf{X}_s, \mathbf{P}_s)$  and  $(\mathbf{X}_r, \mathbf{P}_r)$ , consistent with the event, and the total time also is determined. If the coverage is complete, so that the event uniquely deter-

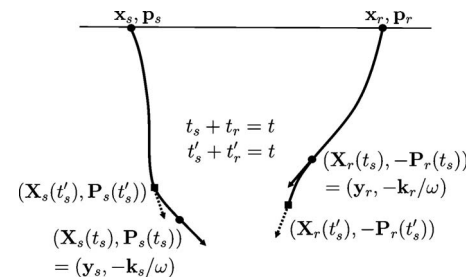


Figure 1. Ray-theoretical relation between data event and double reflector.

mines the source and receiver rays, then the source-receiver representation of the source-receiver reflector must lie along this uniquely determined ray pair. This fact contrasts dramatically with the imaging ambiguities prevalent in all forms of prestack depth migration based on data binning (Nolan and Symes, 1996, 1997; Prucha et al., 1999; Xu et al., 2001; Stolk, 2002; Brandsberg-Dahl et al., 2003; Stolk and Symes, 2004). Even when coverage is complete, in these other forms of prestack migration strong refraction leads to multiple ray pairs connecting data events and reflectors, whence ambiguous imaging of a single event in more than one location within the prestack image volume.

Nonetheless, reflector location still is not uniquely determined by shot-geophone migration, as defined above, for two reasons:

1. Only the total traveltimes is specified by the event! Thus if  $\bar{\mathbf{x}}_s = \mathbf{X}_s(t_s), \bar{\mathbf{x}}_r = \mathbf{X}_r(t_s)$  are related as described above to the event determining the ray pair, so is  $\bar{\mathbf{x}}'_s = \mathbf{X}_s(t'_s), \bar{\mathbf{x}}'_r = \mathbf{X}_r(t'_s)$  with  $t_s + t_r = t'_s + t'_r = t_{sr}$ . See Figure 1.
2. Incomplete acquisition, for example, limited to a narrow azimuth range, might prevent the event from determining its full 3D moveout, as mentioned above. Therefore a family of ray pairs, instead of a unique ray pair, could correspond to the event.

### Kinematics with horizontal subsurface offset

One way to view the remaining imaging ambiguity in shot-geophone migration as defined so far is to recognize that the image point coordinates  $(\bar{\mathbf{x}}, \bar{\mathbf{x}}_s)$  (or  $(\mathbf{x}, \mathbf{h})$ ) are six-dimensional (in three dimensions), whereas the data depend on only five coordinates  $(\mathbf{x}_r, t, \mathbf{x}_s)$  (at most). Formally, restricting one of the coordinates of the image point to be zero at least would make the variable counts equal, so that unambiguous imaging at least would be conceivable. Because physical reflectivities are concentrated at zero (vector) offset, it is natural to restrict one of the offset coordinates to be zero. The conventional choice, beginning with Claerbout's definition of survey-sinking migration (Claerbout, 1985), is the depth coordinate.

We assume that the shot-geophone reflectivity  $R(\mathbf{x}, \mathbf{h})$  takes the form

$$R(\mathbf{x}, \mathbf{h}) = R_z(\mathbf{x}, h_x, h_y) \delta(h_z), \quad (25)$$

leading to the restricted modeling operator:

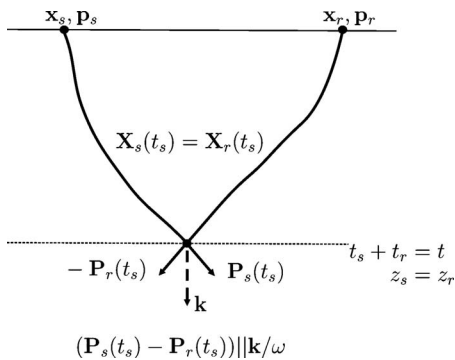


Figure 2. Ray-theoretical relation between data event and physical (single) reflector.

$$\begin{aligned} \bar{F}_z[v]R_z(\mathbf{x}_r, t; \mathbf{x}_s) &= \frac{\partial^2}{\partial t^2} \int d\mathbf{x} \int dh_x \int dh_y R_z(\mathbf{x}, h_x, h_y) \\ &\times \int d\tau G(\mathbf{x} + (h_x, h_y, 0), t - \tau; \mathbf{x}_r) G(\mathbf{x} - (h_x, h_y, 0), \tau; \mathbf{x}_s) \end{aligned} \quad (26)$$

(cf. equations 9 and 10). The kinematics of this restricted operator follows directly from that of the unrestricted operator, developed in the preceding section. Note that equation 25 with the presence of the factor  $\delta(h_z)$  is the natural choice of  $R$  for implementations based on the double-square-root (DSR) equation.

Denote  $\bar{\mathbf{x}}_s = (\bar{x}_s, \bar{y}_s, \bar{z}_s), \mathbf{k}_s = (k_{s,x}, k_{s,y}, k_{s,z})$ , and so on. For horizontal offset, the restricted form of the reflectivity in midpoint-offset coordinates (equation 25) implies a similarly restricted form for its description in sunken source-receiver coordinates:

$$\bar{R}(\bar{\mathbf{x}}_r, \bar{\mathbf{x}}_s) = \bar{R}_z \left( \bar{x}_r, \bar{x}_s, \bar{y}_r, \bar{y}_s, \frac{\bar{z}_r + \bar{z}_s}{2} \right) \delta(\bar{z}_r - \bar{z}_s). \quad (27)$$

Fourier transformation shows that  $\bar{R}$  has a significant plane-wave component with wavenumber  $(\mathbf{k}_r, \mathbf{k}_s)$  precisely when  $\bar{R}_z$  has a significant plane-wave component with wavenumber  $k_{r,x}, k_{r,y}, k_{s,x}, k_{s,y}, (k_{r,z} + k_{s,z})$ . Thus a ray pair  $(\mathbf{X}_r, \mathbf{P}_r), (\mathbf{X}_s, \mathbf{P}_s)$  compatible with a data event with phase space coordinates  $(\mathbf{x}, \mathbf{x}_s, T(\mathbf{x}, \mathbf{x}_s), \omega \mathbf{p}_r, \omega \mathbf{p}_s, \omega)$  images at a point  $X_{r,z}(t_s) = X_{s,z}(t_s) = z$ ,  $P_{r,z}(t_s) - P_{s,z}(t_s) = k_z / \omega$ ,  $X_{s,x}(t_s) = x$ ,  $P_{s,x}(t_s) = k_{s,x} / \omega$ , and so on at image phase space point

$$(\bar{x}_r, \bar{x}_s, \bar{y}_r, \bar{y}_s, z, k_{r,x}, k_{s,x}, k_{r,y}, k_{s,y}, k_z). \quad (28)$$

The adjoint of the modeling operator defined in equation 26 is the horizontal offset shot-geophone migration operator

$$\bar{F}_z^*[v]d(\mathbf{x}, h_x, h_y) = I_{s-g,z}(\mathbf{x}, h_x, h_y), \quad (29)$$

where

$$\begin{aligned} I_{s-g,z}(\mathbf{x}, h_x, h_y) &= \int d\mathbf{x}_r \int d\mathbf{x}_s \int dt \frac{\partial^2}{\partial t^2} d(\mathbf{x}_r, t; \mathbf{x}_s) \\ &\times \int d\tau G(\mathbf{x} + (h_x, h_y, 0), t - \tau; \mathbf{x}_r) G(\mathbf{x} - (h_x, h_y, 0), \tau; \mathbf{x}_s). \end{aligned} \quad (30)$$

As mentioned before, operators and their adjoints enjoy the same kinematic relations, so we have described already the kinematics of this migration operator.

### Semblance property of horizontal offset image gathers and the DSR condition

As explained by Stolk and De Hoop (2001), Claerbout's survey-sinking migration is kinematically equivalent to shot-geophone migration as defined here, under three assumptions: (1) subsurface offsets are restricted to horizontal ( $h_z = 0$ ); (2) rays (either source or receiver) carrying significant energy are nowhere horizontal, i.e.,  $P_{s,z} > 0, P_{r,z} < 0$  throughout the propagation; and (3) events in the data determine full (4D) slowness  $\mathbf{P}_r, \mathbf{P}_s$ .

We call the second condition the "DSR" condition, for reasons explained by Stolk and De Hoop (2001).

*Claim.* Under these restrictions, the imaging operator  $\bar{F}_z^*$  can image a ray pair at precisely one location in image-volume phase space.

When the velocity is correct, the image energy is concentrated therefore at zero offset in the image volume  $I_{s-g,z}$ .

The proof presented by [Stolk and De Hoop \(2001\)](#) uses oscillatory integral representations of the operator  $\bar{F}_z$  and its adjoint. However, the conclusion also follows directly from the kinematic analysis above and the DSR condition.

Indeed, note that the DSR condition implies that depth is increasing along the source ray and decreasing along the receiver ray; otherwise put, depth is increasing along both rays, if you traverse the receiver ray backward. Therefore depth can be used to parameterize the rays. With depth as the parameter, time is increasing from zero along the source ray and decreasing from  $t_r$  along the receiver ray (traversed backward). Thus the two times can be equal (to  $t_s$ ) at exactly one point.

Because the scattering time  $t_s$  is uniquely determined, so are all the other phase space coordinates of the rays. If the ray pair is the incident-reflected ray pair of a reflector, then the reflector must be the only point at which the rays cross because there is only one time  $t_s$  at which  $X_{s,z}(t_s) = X_{r,z}(t_s)$ . See [Figure 3](#). Therefore, in the infinite frequency limit, the energy of this incident-reflected ray pair is imaged at zero offset, consistent with Claerbout's imaging condition.

If, furthermore, coverage is complete, whence the data event uniquely determines the full slowness vectors and hence the rays, then it follows that a data event is imaged at precisely one location, namely the reflector that caused it, and in particular focuses at zero offset. This is the offset version of the result established by [Stolk and De Hoop \(2001\)](#), for which we now have given a different (and more elementary) proof.

### Semblance property of angle image gathers via Radon transform in offset and depth

According to [Sava and Fomel \(2003\)](#), angle image gathers  $A_z$  might be defined via a Radon transform in offset and depth of the off-set image gathers constructed above, i.e., the migrated data volume  $I_{s-g,z}(\mathbf{x}, h_x, h_y)$  (defined in [equation 30](#)) for fixed  $x, y$ :

$$A_z(x, y, \zeta, p_x, p_y) = \int dh_x \int dh_y I_{s-g,z}(x, y, \zeta + p_x h_x + p_y h_y, h_x, h_y), \quad (31)$$

in which  $\zeta$  denotes the  $z$ -intercept parameter, and  $p_x$  and  $p_y$  are the  $x$ - and  $y$ -components of the offset ray parameter. The ray parameter components then might be converted to angle ([Sava and Fomel, 2003; Fomel, 2004; Sava and Fomel, 2005a, 2005b](#)). It follows from this formula that, if the energy in  $I_{s-g,z}(\mathbf{x}, h_x, h_y)$  is focused, i.e., localized, on  $h_x = 0, h_y = 0$ , then the Radon transform  $A_z$  will be (essentially) independent of  $p_x, p_y$ . In other words, when displayed for fixed  $x, y$  with  $\zeta$  axis plotted vertically and  $p_x$  and  $p_y$  horizontally, the events in  $A_z$  will appear flat. The converse is true also. This is the semblance principle for angle gathers.

### SEMBLANCE PROPERTY OF ANGLE GATHERS VIA RADON TRANSFORM IN OFFSET AND TIME

The angle gathers defined by [De Bruin et al. \(1990\)](#) are based on migrated data  $D(\mathbf{x}, h_x, h_y, T)$ , i.e., depending on a time variable  $T$  in addition to the variables  $(\mathbf{x}, h_x, h_y)$ . Such migrated data are given, for example, by the following modification of [equation 30](#):

$$\begin{aligned} D(\mathbf{x}, h_x, h_y, T) &= \int d\mathbf{x}_s \int d\mathbf{x}_r \int dt \frac{\partial^2}{\partial t^2} d(\mathbf{x}_r, t; \mathbf{x}_s) \\ &\times \int d\tau G(\mathbf{x} + (h_x, h_y, 0), t - T - \tau; \mathbf{x}_r) G(\mathbf{x} - (h_x, h_y, 0), \tau; \mathbf{x}_s) \\ &= \int d\mathbf{x}_s \int d\tau u^*(\mathbf{x} + (h_x, h_y, 0), T + \tau; \mathbf{x}_s) \\ &\times (\mathbf{x} - (h_x, h_y, 0), \tau; \mathbf{x}_s) \end{aligned} \quad (32)$$

(which represents a successive evaluation of laterally shifted time correlations accumulated over all shots; cf. [equations 18 and 19](#)). As we have done with other fields, we denote by  $\bar{D}$  the field  $D$  referred to sunken source and receiver coordinates.

Again, this migration formula can be obtained as the adjoint of a modified forward map, mapping an extended reflectivity to data, similarly as above. In this case, the extended reflectivity depends on the variables  $(\mathbf{x}, h_x, h_y, T)$ , with physical reflectivity given by  $r(\mathbf{x})\delta(h_x)\delta(h_y)\delta(T)$ . This physical reflectivity is obtained by a time injection operator,

$$(J_t \bar{R}_z)(\bar{x}_r, \bar{x}_s, \bar{y}_r, \bar{y}_s, \bar{z}, t) = \bar{R}_z(\bar{x}_r, \bar{x}_s, \bar{y}_r, \bar{y}_s, \bar{z}) \delta(t). \quad (33)$$

To obtain a migrated image volume, the extraction of zero-offset data in [equation 14](#) is preceded by extracting the  $T = 0$  data from  $D$ . Setting  $T$  to zero in [equation 32](#) yields the shot-geophone migration output defined in [equation 30](#).

Angle gathers generated via Radon transform in offset and time of  $D(\mathbf{x}, h_x, h_y, T)$  were introduced by [De Bruin et al. \(1990\)](#) and discussed further in [Prucha et al. \(1999\)](#). We denote these gathers by

$$B_z(\mathbf{x}, p_x, p_y) = \int dh_x \int dh_y D(\mathbf{x}, h_x, h_y, p_x h_x + p_y h_y) \chi(h), \quad (34)$$

where  $\chi(h)$  is an appropriately chosen tapered mute restricting the range of  $h$  values ([Stolk and De Hoop, 2001](#)). Angle gathers are obtained upon converting the ray-parameter components to angles ([De Hoop et al., 2003; see also Fomel, 2004](#)).

Note that the Radon transform in [equation 34](#) is evaluated at zero (time) intercept. The dependence on  $z$  is carried by the coordinate plane in which the Radon transform is performed, instead of by the  $(z - )$  intercept as was the case with the angle gathers  $A_z$  defined previously. Note also that  $B_z$  requires the field  $D$ , whereas  $A_z$  might be constructed with the image output.

In [Appendix B](#), we prove that the energy in  $B_z$  is located only at the true scattering point independent of  $(p_x, p_y)$ . Indeed, the semblance

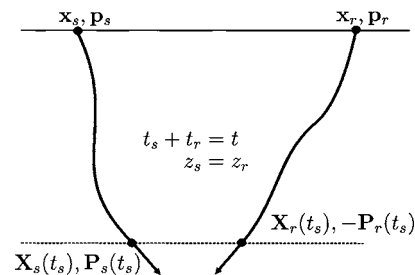


Figure 3. Ray geometry for double reflector with horizontal offset only.

property also holds for the angle transform via Radon transform in the offset time domain, provided that equation B-6 holds.

### Pseudodepth and turning rays

The analysis developed above can be generalized to accommodate a large class of turning rays. To this end, we introduce curvilinear coordinates and the notion of pseudodepth (see Sava and Fomel, 2005a, 2005b), which leads to the curvilinear DSR condition.

In our notation here, we distinguish between horizontal coordinates  $x_\sigma = (x, y)_\sigma$  ( $\sigma = 1, 2$ ) and the vertical coordinate  $z$ . Similarly, the curvilinear coordinates are denoted by  $(\tilde{x}, \tilde{y}, \tilde{z})$ , and we write  $\tilde{x}_\sigma = (\tilde{x}, \tilde{y})_\sigma$  for the ‘‘horizontal’’ coordinates;  $\tilde{z}$  will represent pseudodepth. Our curvilinear coordinates are not connected to the rays associated with the source or receiver Green’s functions; they should reflect the geologic setting.

We need the metric  $\tilde{g}$  associated with the new coordinates. With the original (flat) coordinates, we associate the metric  $g_{ij} = \delta_{jk}$  (we use upper and lower indices as in Riemannian geometry). Then

$$\tilde{g}_{il} = \frac{\partial(x, y, z)^j}{\partial(\tilde{x}, \tilde{y}, \tilde{z})^i} \delta_{jk} \frac{\partial(x, y, z)^k}{\partial(\tilde{x}, \tilde{y}, \tilde{z})^l} \quad (35)$$

with associated volume element  $|\det \tilde{g}|^{1/2} d\tilde{x} d\tilde{y} d\tilde{z} = \left| \frac{\partial(x, y, z)}{\partial(\tilde{x}, \tilde{y}, \tilde{z})} \right| d\tilde{x} d\tilde{y} d\tilde{z}$ . We use the summation convention: summation over repeated indices is implicit (in other words, this equation is a shorthand for  $\tilde{g}_{ii} = \sum_{j,k=1}^3 \frac{\partial(x, y, z)^j}{\partial(\tilde{x}, \tilde{y}, \tilde{z})^i} \delta_{jk} \frac{\partial(x, y, z)^k}{\partial(\tilde{x}, \tilde{y}, \tilde{z})^i}$ ). The inverse metric equals

$$\tilde{g}^{il} = \frac{\partial(\tilde{x}, \tilde{y}, \tilde{z})^i}{\partial(x, y, z)^j} \delta^{jk} \frac{\partial(\tilde{x}, \tilde{y}, \tilde{z})^l}{\partial(x, y, z)^k}. \quad (36)$$

The coordinate  $\tilde{z}$  defines a local pseudodepth if  $\frac{\partial(x, y, z)}{\partial \tilde{x}} \perp \frac{\partial(x, y, z)}{\partial \tilde{z}}$  and  $\frac{\partial(x, y, z)}{\partial \tilde{y}} \perp \frac{\partial(x, y, z)}{\partial \tilde{z}}$ . Thus, the local pseudodepth  $\tilde{z}$  will play a special role, different from  $(\tilde{x}, \tilde{y})$ . We assume that a pseudodepth can be defined at least in target regions, where the metric  $\tilde{g}_{ij}$  must be of the form

$$\tilde{g}_{ij} = \begin{pmatrix} \tilde{g}_{11} & \tilde{g}_{12} & 0 \\ \tilde{g}_{21} & \tilde{g}_{22} & 0 \\ 0 & 0 & \tilde{g}_{33} \end{pmatrix}_{ij}; \quad (37)$$

the inverse metric  $\tilde{g}^{ij}$  is of the same form. In addition,  $\tilde{g}_{\sigma\sigma'}$  denotes the elements of the  $2 \times 2$  matrix

$$\tilde{g}_{\sigma\sigma'} = \begin{pmatrix} \tilde{g}_{11} & \tilde{g}_{12} \\ \tilde{g}_{21} & \tilde{g}_{22} \end{pmatrix}_{\sigma\sigma'}, \quad (38)$$

i.e., the horizontal part of the metric. For our analysis, we need only local coordinates and a Riemannian metric of the form 37.

The transformation of the acoustic wave equation is done most naturally using a variational formulation. This yields an action functional

$$S = \frac{1}{2} \int_a^b \int \int \left( \kappa \left| \frac{\partial u}{\partial t} \right|^2 - \rho^{-1} \|\nabla u\|^2 + uf \right) dx dy dz dt, \quad (39)$$

where  $\rho$  is the density, and  $\kappa$  is the compressibility whence  $c^{-2} = \rho\kappa$ . The wave equation follows from the Euler-Lagrange equations derived from this action. The variation of this action under  $v$  (the derivative if  $u \rightarrow u + v$ ) can be written as

$$\begin{aligned} \delta_v S &= \int_a^b \int \int \left( \kappa \frac{\partial v}{\partial t} \frac{\partial u}{\partial t} - \rho^{-1} \nabla v \cdot \nabla u + vf \right) dx dy dz dt \\ &= \int_a^b \int \int v \left( -\kappa \frac{\partial^2 u}{\partial t^2} + \nabla \cdot (\rho^{-1} \nabla u) + f \right) dx dy dz dt, \end{aligned} \quad (40)$$

where the second step was obtained by integration by parts, using that  $v = 0$  for  $t = a$  and  $t = b$ . Because this must be true for all  $v$ , the wave equation follows.

We define the transformed wavefield as  $\tilde{u}(\tilde{x}, \tilde{y}, \tilde{z}) = u(x(\tilde{x}, \tilde{y}, \tilde{z}), y(\tilde{x}, \tilde{y}, \tilde{z}), z(\tilde{x}, \tilde{y}, \tilde{z}))$ . To obtain the wave equation in the new coordinates (see also Friedlander, 1976), we transform the action. In the new coordinates, it becomes

$$\begin{aligned} S &= \frac{1}{2} \int_a^b \int \int \left[ \kappa \left| \frac{\partial \tilde{u}}{\partial t} \right|^2 \right. \\ &\quad \left. - \rho^{-1} \left( \frac{\partial(\tilde{x}, \tilde{y}, \tilde{z})}{\partial(x, y, z)} \frac{\partial \tilde{u}}{\partial(\tilde{x}, \tilde{y}, \tilde{z})} \right) \cdot \left( \frac{\partial(\tilde{x}, \tilde{y}, \tilde{z})}{\partial(x, y, z)} \frac{\partial \tilde{u}}{\partial(\tilde{x}, \tilde{y}, \tilde{z})} \right) + \tilde{u}f \right] \\ &\quad \times \left| \frac{\partial(x, y, z)}{\partial(\tilde{x}, \tilde{y}, \tilde{z})} \right| d\tilde{x} d\tilde{y} d\tilde{z} dt. \end{aligned} \quad (41)$$

By an argument similar to that above, it follows that the wave equation has new coefficients (which now are anisotropic),  $\kappa \left| \frac{\partial(x, y, z)}{\partial(\tilde{x}, \tilde{y}, \tilde{z})} \right|$  and  $\rho^{-1} \left| \frac{\partial(x, y, z)}{\partial(\tilde{x}, \tilde{y}, \tilde{z})} \right| \tilde{g}^{ij}$ , and reads

$$\begin{aligned} \kappa \left| \frac{\partial(x, y, z)}{\partial(\tilde{x}, \tilde{y}, \tilde{z})} \right| \frac{\partial^2 \tilde{u}}{\partial t^2} - \frac{\partial}{\partial(\tilde{x}, \tilde{y}, \tilde{z})^i} \left( \rho^{-1} \left| \frac{\partial(x, y, z)}{\partial(\tilde{x}, \tilde{y}, \tilde{z})} \right| \tilde{g}^{ij} \frac{\partial \tilde{u}}{\partial(\tilde{x}, \tilde{y}, \tilde{z})^j} \right) \\ = f \left| \frac{\partial(x, y, z)}{\partial(\tilde{x}, \tilde{y}, \tilde{z})} \right| \end{aligned} \quad (42)$$

or

$$\begin{aligned} \kappa \left| \frac{\partial(x, y, z)}{\partial(\tilde{x}, \tilde{y}, \tilde{z})} \right| \frac{\partial^2 \tilde{u}}{\partial t^2} - \frac{\partial}{\partial \tilde{z}} \left( \alpha \frac{\partial \tilde{u}}{\partial \tilde{z}} \right) \\ - \frac{\partial}{\partial \tilde{x}^\sigma} \left( \rho^{-1} \left| \frac{\partial(x, y, z)}{\partial(\tilde{x}, \tilde{y}, \tilde{z})} \right| \tilde{g}^{\sigma\sigma'} \frac{\partial \tilde{u}}{\partial \tilde{x}^{\sigma'}} \right) = f \left| \frac{\partial(x, y, z)}{\partial(\tilde{x}, \tilde{y}, \tilde{z})} \right|, \end{aligned} \quad (43)$$

with  $\alpha = \rho^{-1} \tilde{g}^{33} \left| \frac{\partial(x, y, z)}{\partial(\tilde{x}, \tilde{y}, \tilde{z})} \right|$ . In the case of flat coordinates, assuming that  $\rho$  is constant, the Green’s function (cf. equation 1) satisfies equation 43 subject to the substitution  $f = \rho \delta(\mathbf{x} - \mathbf{x}_s) \delta(t)$ .

Asymptotic ray theory corresponding with the solutions of equation 42 is governed by the Hamiltonian  $\mathcal{H}$ , obtained from the symbol of the wave operator on the left-hand side, which in curvilinear coordinates is given by

$$\begin{aligned} \mathcal{H}(\tilde{x}, \tilde{y}, \tilde{z}, \tilde{p}_x, \tilde{p}_y, \tilde{p}_z) &= \frac{1}{2}(\tilde{p}_x, \tilde{p}_y, \tilde{p}_z) i \tilde{g}^{ij} \\ &\times c^2(x(\tilde{x}, \tilde{y}, \tilde{z}), y(\tilde{x}, \tilde{y}, \tilde{z}), z(\tilde{x}, \tilde{y}, \tilde{z}))(\tilde{p}_x, \tilde{p}_y, \tilde{p}_z)_j, \quad c^2 = (\rho \kappa)^{-1}; \end{aligned} \quad (44)$$

here,  $(\tilde{p}_x, \tilde{p}_y, \tilde{p}_z)$  are the components of a slowness vector in curvilinear coordinates. Singularities propagate along rays, with tangent, or velocity, vectors given by

$$(\tilde{v}_x(t), \tilde{v}_y(t), \tilde{v}_z(t)) = \frac{d\tilde{\mathbf{X}}}{dt} = -\frac{\partial \mathcal{H}}{\partial (\tilde{p}_x, \tilde{p}_y, \tilde{p}_z)}. \quad (45)$$

Where the Riemannian metric attains the form 37, the  $\tilde{x}$ -velocity satisfies

$$\tilde{v}^\sigma(t) = c^2 \tilde{g}^{\sigma\sigma'} \tilde{P}_{\sigma'}, \quad (46)$$

expressing the relation between group velocities and slowness vectors. Moreover,

$$\frac{d\tilde{\mathbf{P}}}{dt} = \frac{\partial \mathcal{H}}{\partial (\tilde{x}, \tilde{y}, \tilde{z})}, \quad (47)$$

and the length of the slowness vector is such that  $\mathcal{H}(\tilde{x}, \tilde{y}, \tilde{z}, \tilde{p}_x, \tilde{p}_y, \tilde{p}_z) = \frac{1}{2}$ .

Equation 34 is replaced by

$$B_z(\tilde{x}, \tilde{y}, \tilde{z}, \tilde{p}_x, \tilde{p}_y) = \int dS(\tilde{h}_x, \tilde{h}_y) \tilde{D}(\tilde{x}, \tilde{y}, \tilde{z}, \tilde{h}_x, \tilde{h}_y, \tilde{p}_\sigma \tilde{h}^\sigma) \chi(\tilde{h}_x, \tilde{h}_y), \quad (48)$$

where

$$dS(\tilde{h}_x, \tilde{h}_y) = |j(\tilde{h}_x, \tilde{h}_y)^T j(\tilde{h}_x, \tilde{h}_y)|^{1/2} d\tilde{h}_x d\tilde{h}_y, \quad (49)$$

in which

$$\begin{aligned} j(\tilde{h}_x, \tilde{h}_y) &= \frac{\partial(\mathbf{x}_s, \mathbf{x}_r)}{\partial(\tilde{h}_x, \tilde{h}_y)}, \quad \mathbf{x}_s = \mathbf{x}_s(\tilde{x} - \tilde{h}_x, \tilde{y} - \tilde{h}_y, \tilde{z}), \\ &= \tilde{\mathbf{x}}_s \\ \mathbf{x}_r &= \mathbf{x}_r(\tilde{x} + \tilde{h}_x, \tilde{y} + \tilde{h}_y, \tilde{z}) \\ &= \tilde{\mathbf{x}}_r \end{aligned} \quad (50)$$

using that  $\tilde{z}$  is a pseudodepth. We now assume that the source and receiver rays become nowhere horizontal in the curvilinear coordinate system. We refer to this assumption as the curvilinear DSR condition. An example of a violation of this condition, which leads to the generation of artifacts, is illustrated in Figure 4.

In Appendix B, we prove that the energy in the angle transform defined in equation 48 is located only at the true scattering point independent of  $\tilde{p}$ .

### EXAMPLE

We illustrate the semblance property established in the preceding pages for shot-geophone migration. In an example containing a low velocity lens, we expose the dramatic contrast between image (or common-image-point) gathers produced by shot-geophone migration and those produced by other forms of prestack depth migration.

The formation of caustics leads to failure of the semblance principle for Kirchhoff (or generalized Radon transform) common-scattering-angle migration. The DSR assumption is satisfied for the acquisition offsets considered. For the shot-geophone migration, we use a method based on solving Helmholtz equations (Sirgue and Pratt, 2004): we use a fourth-order finite-difference scheme in space and apply second-order absorbing boundary conditions. We form angle image gathers according to equation 34.

The example is used in Stolk (2002) and Stolk and Symes (2004) to show that common-offset and Kirchhoff (or generalized Radon transform) common-scattering-angle migration produce strong kinematic artifacts in strongly refracting velocity models. The velocity model (Figure 5) consists of a slow Gaussian lens embedded in a constant background. This model is strongly refracting through the formation of triplications in the ray fields. Below the lens, at a depth of 2 km, we placed a flat, horizontal reflector. We synthesized data using a (4-,10-,20-,40-) Hz zero-phase band-pass filter as (isotropic) source wavelet, and a (centered) finite-difference scheme — of order 2 in time and 4 in space, with perfectly matched layer (PML) absorbing boundary conditions all around — with adequate sampling. A typical shot gather over the lens (Figure 6, shot position at –500 m) shows a complex pattern of reflections, from the flat reflector, that have propagated through the lens.

We migrated the data with the above-mentioned approach. Figure 7 shows the image, which clearly reproduces the reflector. An angle image gather is shown in Figure 8; for comparison, we show the Kirchhoff common-scattering-angle image gather in Figure 9 at the same location (reproduced from Stolk and Symes, 2004), each trace of which is obtained by Kirchhoff migration restricted to common angle. The Kirchhoff image gather clearly is contaminated by numerous energetic nonflat events, whereas the wave-equation image gather is not. The geometry of these artifacts is computed directly and indicated by solid lines. Artifacts in the Kirchhoff image gather must be nonflat and can be removed by “dip” filtering in depth and angle, but only if the velocity model is perfectly well known.

For comparison, we generated a source image gather via reverse time migration at the same location as the other two image gathers;

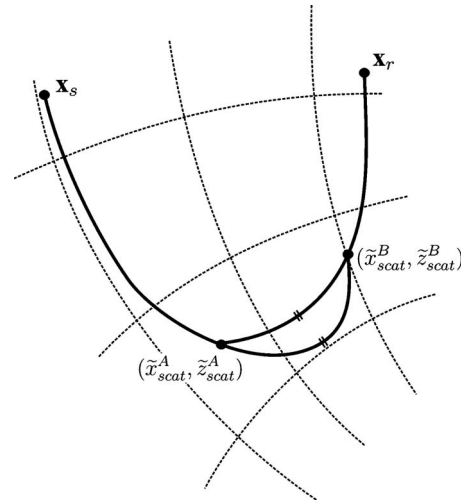


Figure 4. Violation of the curvilinear DSR condition leading to the generation of artifacts in the angle gathers. The traveltimes associated with the ray segments indicated by  $\parallel$  are equal, and the imaging ambiguity here occurs between points  $(\tilde{x}_{scat}^A, \tilde{z}_{scat}^A)$  and  $(\tilde{x}_{scat}^B, \tilde{z}_{scat}^B)$ .

see Figure 10. We note, again, the presence of artifacts now computed with a wave-equation approach, but with a different geometry because common-source and common-angle restrictions imply the use of different data subsets. However, the appearance of the artifacts in both cases is very similar.

**DISCUSSION**

The literature contains some comparisons of Kirchhoff and wave equation migration (e.g., Albertin et al., 2002; Fliedner et al., 2002).

Performance differences identified in these reports have been ascribed to a wide variety of factors, such as differences in antialiasing and decimation strategies, choice of time fields used in Kirchhoff imaging, and “fidelity” to the wave equation. These factors surely affect performance, but they reflect mainly implementation decisions. The difference identified and demonstrated in this study, on the other hand, is fundamental: it flows from the differing formulations of prestack imaging (and modeling) underlying the two classes of methods. No implementation variations can mask it.

From a processing or data flow point of view, the (wave-equation) angle transform generating image gathers via Radon transform in subsurface offset and time distinguishes itself from common-angle (Kirchhoff) migration through (curvilinear) survey sinking applied to all the data prior to forming angle gathers in the subsurface instead of restricting the surface data (in a velocity-field-dependent manner).

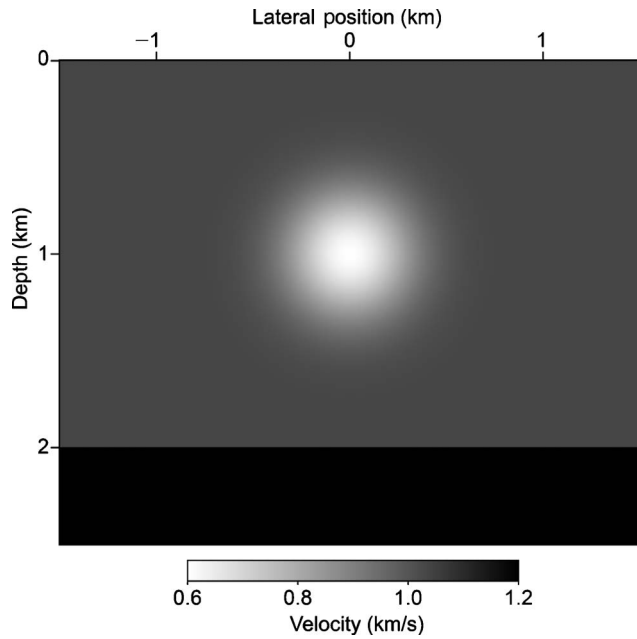


Figure 5. Lens velocity model over flat reflector.

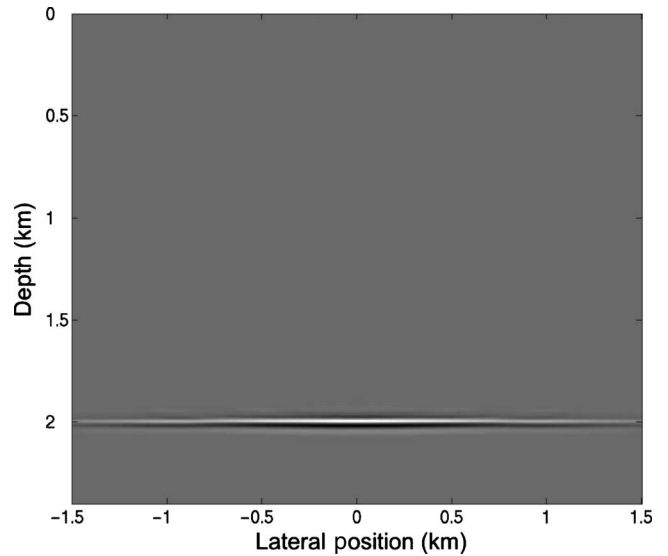


Figure 7. Wave equation image of the flat reflector using all the data generated over the lens model illustrated in Figure 5.

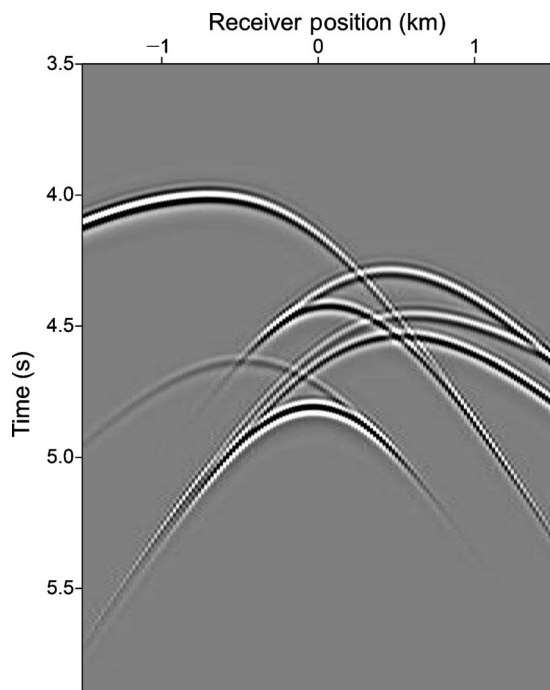


Figure 6. Lens model, shot record at shot location  $-0.5$  km.

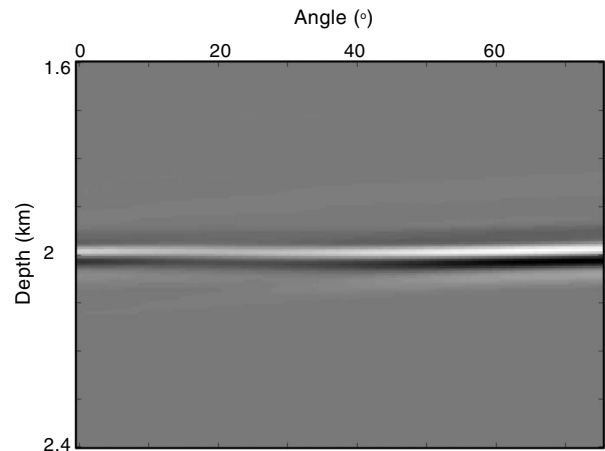


Figure 8. Lens model, common-image-point gather obtained with the wave-equation angle transform at  $x_m = 0.3$  km.

The idea of using nonhorizontal subsurface offset while forming common-image-point gathers has been explored quite recently. Numerical investigations of Biondi and Shan (2002) suggest that reverse-time (two-way) wave equation migration, as presented here, could be modified by inclusion of nonhorizontal offsets to permit the use of turning energy, and indeed to image reflectors of arbitrary dip. This latter possibility has been understood in the context of (stacked) images for some time (Yoon et al., 2003). Biondi and Shan (2002) present prestack image gathers for horizontal and vertical offsets, which suggest that a similar flexibility might be available for the shot-geophone extension.

Biondi and Symes (2004) give a local analysis of shot-geophone image formation using nonhorizontal offsets. Globally the formation of kinematic artifacts in a horizontal/vertical offset image volume cannot be entirely ruled out; however, kinematic artifacts cannot occur at arbitrarily small offset, in contrast to the formation of artifacts at all offsets in binwise migration. Here, we have provided a rigorous framework with general subsurface offsets upon introducing curvilinear coordinates for incorporating “turning rays” while

preserving the semblance property of angle gathers.

The “enough-data” condition listed in the introduction and assumed throughout this study is an important one. For arbitrary 3D complexity in the migration velocity field, validity of the semblance principle requires areal coverage (“true 3D” data). In particular, we cannot guarantee the absence of kinematic artifacts in shot-geophone migration of narrow-azimuth data unless the velocity model is assumed to have additional properties, for example, mild crossline heterogeneity, which compensate to some extent for the lack of azimuths. This issue is discussed a bit more in the concluding section.

An intriguing and so far theoretically untouched area concerns the potential of multiple narrow-azimuth surveys, with distinct central azimuths, to resolve the ambiguities of single-azimuth imaging.

True-amplitude adaptations of shot-geophone migration and the generation of angle image gathers, based on the one-way wave equation, are developed in the literature; see Stolk and De Hoop (2001, 2006), De Hoop (2004), Joncour et al. (2005), and Zhang et al. (2007).

## CONCLUSION

We have demonstrated, mathematically and by example, that shot-geophone migration produces artifact-free image volumes, assuming (1) a kinematically correct and relatively smooth velocity model, (2) a (local) curvilinear coordinate system and an associated Riemannian metric admitting the introduction of pseudodepth with respect to which incident energy travels “downward” and reflected energy travels “upward,” and (3) enough data to uniquely determine rays corresponding to events in the data. In an example, we compared shot-geophone migration with Kirchhoff common-scattering-angle migration. Although the latter technique bins data only implicitly, it is like other binwise migration schemes, such as common-offset migration, in generating kinematic image artifacts in prestack data when the velocity model is sufficiently complex to strongly refract waves.

We have shown that implementation has, at most, a secondary impact on kinematic accuracy of shot-geophone imaging. Its basic kinematics is shared not just by the two common-depth-extrapolation implementations — shot profile, double square root — but also by a variant of reverse time imaging and even by a Kirchhoff or generalized Radon transform operator of appropriate construction. Naturally these various options differ in numerous ways, in their demands on data quality and sampling and in their sensitivity to various types of numerical artifacts. However, in the ideal limit of continuous data and discretization-free computation, all share an underlying kinematic structure and offer the potential of artifact-free data volumes when the assumptions of our theory are satisfied, even in the presence of strong refraction and multiple arrivals at reflecting horizons.

It remains to address three shortcomings of the theory. The first is its reliance on a (local) curvilinear coordinate system and corresponding “DSR” assumption. This restricts the class of allowable “turning rays” (but reflections off a vertical salt flank, where pseudodepth becomes close to horizontal, can satisfy this assumption).

A second limitation of our main result is the assumption that ray kinematics is determined completely by the data. Of course, this is no limitation for the 2D synthetic examples presented above. With the advent of WATS acquisition, this limitation is overcome as well. However, most contemporary data are acquired with narrow-azimuth streamer equipment. For such data, we cannot in general rule

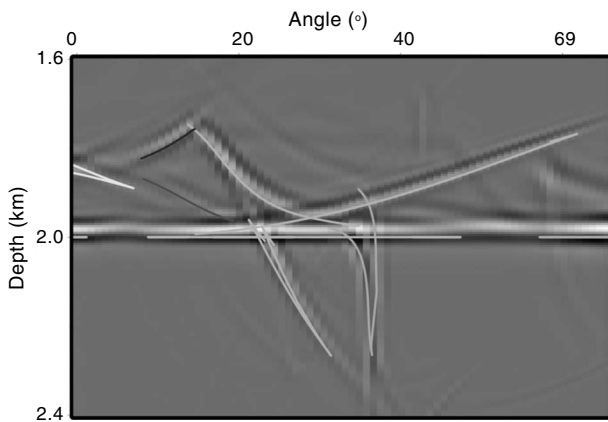


Figure 9. Lens model, common-image-point gather obtained with the Kirchhoff angle transform at  $x_m = 0.3$  km. The curves in gray indicate the different kinematic artifacts as predicted by ray-based computations, all of which have residual moveout.

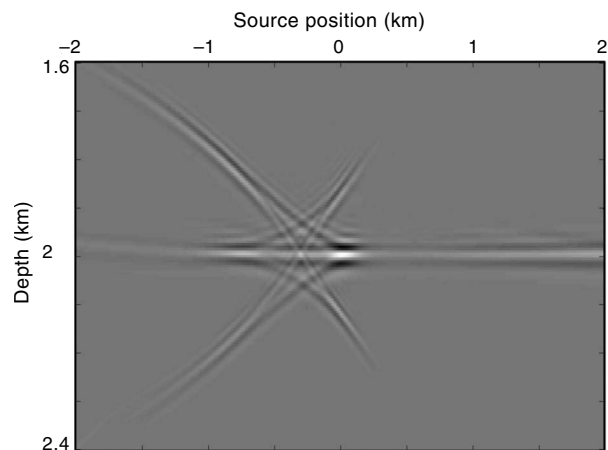


Figure 10. Lens model, source common-image-point gather obtained via reverse time migration at  $x_m = 0.3$  km.

out the appearance of artifacts resulting from multiple ray pairs satisfying the shot-geophone kinematic imaging conditions.

However, two observations suggest that all is not lost in this situation. First, for an ideal “2.5D” structure (independent of a crossline coordinate) and perfect linear survey geometry (no feathering), all energetic rays remain in the vertical planes through the sail line, and our analysis applies without alteration to guarantee imaging fidelity. Second, the conditions that ensure absence of artifacts are open; i.e., small perturbations of velocity and source and receiver locations cannot affect the conclusion. Therefore, shot-geophone imaging fidelity is robust against mild crossline heterogeneity and small amounts of cable feathering. Note that nothing about the formulation of our modeling or (adjoint) migration operators requires areal geometry: the operators are perfectly well defined for narrow-azimuth data.

A third, and much more fundamental, limitation pertains to migration itself. Migration operators are essentially adjoints to linearized modeling operators. The kinematic theory of migration requires that the velocity model be slowly varying on the wavelength scale, or at best be slowly varying except for a discrete set of fixed, regular interfaces. The most challenging contemporary imaging problems, for example, subsalt prospect assessment, transgress this limitation, in many cases violently. Salt-sediment interfaces are among the unknowns, especially bottom salt, are quite irregular, and are perhaps not even truly interfaces. Clever solutions are being devised for these difficult imaging problems, but the theory lags far, far behind the practice.

## ACKNOWLEDGMENTS

This work was supported in part by the National Science Foundation and by the sponsors of The Rice Inversion Project (TRIP). MdH also acknowledges support by the members of the Geo-Mathematical Imaging Group (GMIG). CCS acknowledges support from the Netherlands Organization for Scientific Research (now) under grant no. 639.032.509. We thank Shen Wang for his help in generating the examples, Norman Bleistein for careful scrutiny of an early draft, and Sergey Fomel for many valuable comments.

## APPENDIX A

### REFLECTIONS TO REFLECTORS

In this appendix, we establish the relation between the appearance of events in the data and the presence of reflectors in the migrated image. This relation is the same for the forward modeling operator and for its adjoint, the migration operator.

The reasoning presented here shares with [Stolk and De Hoop \(2001\)](#) the identification of events, respectively reflectors, by high-frequency asymptotics in phase space, but differs in that it does not explicitly use oscillatory integral representations of  $F[v]$ . Instead, this argument follows the pattern of [Rakesh’s analysis of shot-profile-migration kinematics \(Rakesh, 1988\)](#). It can be made mathematically rigorous by means of the so-called Gabor calculus in the harmonic analysis of singularities ([Duistermaat, 1973](#), chap. 1).

Our analysis is based on the recognition that the shot-geophone predicted data field  $u(\mathbf{x}_r, t; \mathbf{x}_s)$ , defined by equation 10, is the value at  $\bar{\mathbf{x}} = \mathbf{x}_r$  of the space-time field  $u(\bar{\mathbf{x}}, t; \mathbf{x}_s)$ , which solves

$$\begin{aligned} & \frac{1}{v^2(\bar{\mathbf{x}})} \frac{\partial^2 u}{\partial t^2}(\bar{\mathbf{x}}, t; \mathbf{x}_s) - \nabla_{\bar{\mathbf{x}}}^2 u(\bar{\mathbf{x}}, t; \mathbf{x}_s) \\ &= \int d\mathbf{h} R(\bar{\mathbf{x}} - \mathbf{h}, \mathbf{h}) \frac{\partial^2}{\partial t^2} G(\bar{\mathbf{x}} - 2\mathbf{h}, t; \mathbf{x}_s). \end{aligned} \quad (\text{A-1})$$

This equation follows directly by applying the wave operator to both sides of equation 10.

The appearance of an event at a point  $(\mathbf{x}_s, \mathbf{x}_r, t_{sr})$  in the data volume is equivalent to the presence of a sizable Fourier coefficient for a plane-wave component

$$e^{i\omega(t - \mathbf{p}_s \bar{\mathbf{x}}_s - \mathbf{p}_r \bar{\mathbf{x}}_r)} \quad (\text{A-2})$$

in the acoustic field for frequencies  $\omega$  within the bandwidth of the data, even after muting out all events at a small distance from  $(\mathbf{x}_s, \mathbf{x}_r, t_{sr})$ .

Note that the data does not necessarily fully determine this plane-wave component, i.e., the full 3D event slownesses  $\mathbf{p}_s, \mathbf{p}_r$ . In this appendix,  $\mathbf{p}_s, \mathbf{p}_r$  are assumed to be compatible with the data in the sense just explained.

Assume that these frequencies are high enough relative to the length scales in the velocity so that such local plane-wave components propagate according to geometric acoustics. This assumption tacitly underlies much of reflection processing, and in particular is vital to the success of migration.

In other words, solutions of wave equations such as A-1 carry energy in local plane-wave components along rays. Let  $(\mathbf{X}_r(t), \mathbf{P}_r(t))$  denote such a ray, so that  $\mathbf{X}_r(t_{sr}) = \mathbf{x}_r, \mathbf{P}_r(t_{sr}) = \mathbf{p}_r$ . Then at some point, the ray must pass through a point in phase space at which the source term (right-hand side) of equation A-1 has significant energy. Otherwise, the ray never would pick up any energy at all, and there would be no event at time  $t_{sr}$ , receiver position  $\mathbf{x}_r$ , and receiver slowness  $\mathbf{p}_r$ . (Supplemented with proper mathematical boilerplate, this statement is the celebrated propagation of singularities theorem of Hörmander [[Taylor, 1981; Hormander, 1983](#)].)

The source term involves a product and an integral in some of the variables. The Green’s function  $G(\bar{\mathbf{x}}_s, t, \mathbf{x}_s)$  has high-frequency components along rays from the source, i.e., at points of the form  $(\mathbf{X}_s(t_s), \mathbf{P}_s(t_s))$ , where  $\mathbf{X}_s(0) = \mathbf{x}_s$  and  $t_s \geq 0$ . (Of course, this is just another instance of the propagation of singularities, as the source term in the wave equation for  $G(\bar{\mathbf{x}}_s, t, \mathbf{x}_s)$  is singular only at  $(\mathbf{x}_s, 0)$ .) In other words, viewed as a function of  $\bar{\mathbf{x}}_s$  and  $t_s$ ,  $G(\cdot, \cdot; \mathbf{x}_s)$  will have significant Fourier coefficients for plane waves

$$e^{i\omega(\mathbf{P}_s(t_s) \bar{\mathbf{x}}_s + t_s)}. \quad (\text{A-3})$$

We characterize reflectors in the same way, i.e., there is a (double) reflector at  $(\bar{\mathbf{x}}_s, \bar{\mathbf{x}}_r)$  if  $\bar{R}$  has significant Fourier coefficients of a plane wave

$$e^{i(\mathbf{k}_s \bar{\mathbf{x}}_s' + \mathbf{k}_r \bar{\mathbf{x}}_r')} \quad (\text{A-4})$$

for some pair of wavenumbers  $\mathbf{k}_s, \mathbf{k}_r$ , and for generic points  $(\bar{\mathbf{x}}_s', \bar{\mathbf{x}}_r')$  near  $(\bar{\mathbf{x}}_s, \bar{\mathbf{x}}_r)$ . Presumably then, the product  $R(\bar{\mathbf{x}}_s', \mathbf{x}) G(\bar{\mathbf{x}}_s', t_s; \mathbf{x}_s)$  has a significant coefficient of the plane-wave component

$$e^{i((\mathbf{k}_s + \omega \mathbf{P}_s(t_s)) \bar{\mathbf{x}}_s' + \mathbf{k}_r \mathbf{x} + \omega t_s)} \quad (\text{A-5})$$

for  $\bar{\mathbf{x}}_s'$  near  $\bar{\mathbf{x}}_s$ ,  $\mathbf{x}$  near  $\bar{\mathbf{x}}_r$ ; note that implicitly we have assumed that  $\bar{\mathbf{x}}_s$  (the argument of  $G$ ) is located on a ray from the source with time  $t_s$ . The right-hand side of equation A-1 integrates this product over  $\bar{\mathbf{x}}_s$ .

This integral will be negligible unless the phase in  $\bar{\mathbf{x}}_s$  is stationary; that is, to produce a substantial contribution to the right-hand side of equation A-1, it is necessary that

$$\bar{\mathbf{x}}_s = \mathbf{X}_s(t_s), \quad \mathbf{k}_s + \omega \mathbf{P}_s(t_s) = 0. \quad (\text{A-6})$$

Supposing that this is so, the remaining exponential suggests that the right-hand side of equation A-1 has a sizable passband component of the form

$$e^{i(\mathbf{k}_r \cdot \mathbf{x} + \omega t_s)} \quad (\text{A-7})$$

for  $\mathbf{x}$  near  $\bar{\mathbf{x}}_r$ . As argued above, this right-hand side will give rise to a significant plane-wave component in the solution  $u$  arriving at  $\mathbf{x}_r$  at time  $t_{sr} = t_s + t_r$  exactly when a ray arriving at  $\mathbf{x}_r$  at time  $t_{sr}$  starts from a position in space-time with the location and wavenumber of this plane wave, at time  $t_s = t_{sr} - t_r$ ; i.e.,

$$\mathbf{X}_r(t_s) = \bar{\mathbf{x}}_r, \quad \omega \mathbf{P}_r(t_s) = \mathbf{k}_r. \quad (\text{A-8})$$

We end this appendix with a remark about the case of complete coverage; i.e., sources and receivers densely sample a fully 2D area on or near the surface. Assuming that the effect of the free surface has been removed so that all events might be viewed as samplings of an upcoming wavefield, the data (2D) event slowness uniquely determines the wavefield (3D) slowness through the eikonal equation. Thus an event in the data is characterized by its (3D) moveout: locally, by a moveout equation  $t = T(\mathbf{x}_s, \mathbf{x}_r)$ , and infinitesimally by the source and receiver slownesses

$$\mathbf{p}_s = \nabla_{\mathbf{x}_s} T, \quad \mathbf{p}_r = \nabla_{\mathbf{x}_r} T. \quad (\text{A-9})$$

In this case, the data event uniquely determines the source and receiver rays.

## APPENDIX B

### PROOF OF SEMBLANCE PROPERTY

In this appendix, we prove the semblance property of angle gathers via Radon transform in offset and time.

#### Formulation in “global” depth

Our starting point is equation 34 combined with equation 32. We first need to establish at which points  $(\mathbf{x}, h_x, h_y, T)$  significant energy of  $D(\mathbf{x}, h_x, h_y, T)$  is located. The argument for  $\bar{D}$  is slightly different from the argument for  $\bar{I}_{s-g,z}$  because  $\bar{D}$  depends also on the time. For  $\bar{I}_{s-g,z}$ , there was a kinematic relation  $(\mathbf{x}_s, \mathbf{x}_r, t_{sr}, \omega \mathbf{p}_s, \omega \mathbf{p}_r, \omega)$  to a point in phase space  $(x_s, x_r, y_s, y_r, z, k_{s,x}, k_{r,x}, k_{s,y}, k_{r,y}, k_z)$  where the energy in  $\bar{I}_{s-g,z}$  is located. The restriction of  $\bar{D}$  to time  $T$  is the same as the restriction to time 0, but using time-shifted data  $d(\cdot, t + T, \cdot)$ . Therefore we can follow almost the same argument as for the kinematic relation of  $\bar{I}_{s-g,z}$ .

We find that for an event at  $(\mathbf{x}_s, \mathbf{x}_r, t_{sr}, \omega \mathbf{p}_s, \omega \mathbf{p}_r, \omega)$  to contribute at  $\bar{D}$ , restricted to time  $T$ , we must have  $(x_s, y_s, z)$  on the ray  $\mathbf{X}_s$ , say, at time  $t'_s$ , i.e.,  $(x_s, y_s, z) = \mathbf{X}_s(t'_s)$ . Then  $(x_r, y_r, z)$  must be on the ray  $\mathbf{X}_r$ , say, at time  $t''_s$ , i.e.,  $(x_r, y_r, z) = \mathbf{X}_r(t''_s)$ . The situation is displayed in Figure B-1, using midpoint-offset coordinates. Furthermore, the sum of the traveltimes from  $\mathbf{x}_s$  to  $(x_s, y_s, z)$  and from  $\mathbf{x}_r$  to  $(x_r, y_r, z)$  must be equal to  $t_{sr} - T$ . It follows that  $t''_s - t'_s = T$ .

Now consider an event from a physical reflection at  $\mathbf{X}_s(t_s) = \mathbf{X}_r(t_s) = (x_{scat}, y_{scat}, z_{scat})$ . We use the previous reasoning to find

where the energy in  $D$  is located (in midpoint-offset coordinates). We denote by  $(v_{s,x}(t), v_{s,y}(t), v_{s,z}(t))$  the ray velocity for the source ray  $\frac{d\mathbf{X}_s}{dt}$ . The horizontal “sunken source” coordinates  $(x - h_x, y - h_y)$  then satisfy

$$x_{scat} - (x - h_x) = \int_{t'_s}^{t_s} dt v_{s,x}(t), \quad (\text{B-1})$$

$$y_{scat} - (y - h_y) = \int_{t'_s}^{t_s} dt v_{s,y}(t).$$

or the “sunken receiver” coordinates, we find

$$(x + h_x) - x_{scat} = \int_{t_s}^{t''_s} dt v_{r,x}(t), \quad (\text{B-2})$$

$$(y + h_y) - y_{scat} = \int_{t_s}^{t''_s} dt v_{r,y}(t).$$

Adding up the  $x$ -components of these equations, and separately the  $y$ -components of these equations, gives

$$2h_x = \int_{t'_s}^{t''_s} v_x(t) dt, \quad 2h_y = \int_{t'_s}^{t''_s} v_y(t) dt, \quad (\text{B-3})$$

where now the velocity  $(v_x(t), v_y(t))$  is from the source ray for  $t < t_s$ , and from the receiver ray for  $t > t_s$ . Let us denote by  $v_{\parallel, \max}$  the maximal horizontal velocity along the rays between  $(x_{scat}, y_{scat}, z_{scat})$  and the points  $(x_s, y_s, z)$  and  $(x_r, y_r, z)$ ; then we have

$$2\|(h_x, h_y)\| \leq |t''_s - t'_s| v_{\parallel, \max} = |T| v_{\parallel, \max}. \quad (\text{B-4})$$

For the 2D case, we display the situation in Figure B-2. The energy in  $\bar{D}$  is located in the shaded region of the  $(h_x, T)$  plane indicated in this figure. In three dimensions, this region becomes a cone.

The angle transform in equation 34 is an integral of  $D$  over a plane in the  $(h_x, h_y, T)$  volume given by

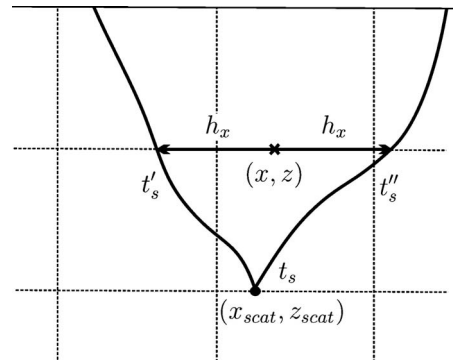


Figure B-1. Ray geometry for offset-time angle-gather construction

$$T = p_x h_x + p_y h_y. \quad (\text{B-5})$$

Suppose now that

$$\sqrt{p_x^2 + p_y^2} < \frac{2}{v_{\parallel, \max}}. \quad (\text{B-6})$$

Then we have

$$|T| = |p_x h_x + p_y h_y| < \frac{2}{v_{\parallel, \max}} \sqrt{h_x^2 + h_y^2}. \quad (\text{B-7})$$

In Figure B-2 (the 2D case), this means that the lines of integration are not in the shaded region of the  $(h_x, T)$  plane. In three dimensions, the planes of integration are not in the corresponding cone. The only points where the planes of integration intersect the set of  $(h_x, h_y, T)$ , where energy of  $D$  is located, are points with  $T = 0$ ,  $h_x = h_y = 0$ . It follows that the energy in the angle transform of equation 34 is located only at the true scattering point independent of  $(p_x, p_y)$ . We conclude that the semblance property also holds for the angle transform via Radon transform in the offset time domain, provided that B-6 holds.

The bound  $v_{\parallel, \max}$  need not be a global bound on the horizontal component of the ray velocity. The integral in equation 34 is over some finite range of offsets, hence on some finite range of times, so that the distance between, say, the midpoint  $\mathbf{x}$  in equation 34 and the physical scattering point is bounded. Therefore,  $v_{\parallel, \max}$  should be a bound on the horizontal component of the ray velocity on some sufficiently large region around  $\mathbf{x}$ .

### Formulation in (local) pseudodepth

We adapt the analysis presented in the previous subsection to the case of curvilinear coordinates defining a metric with a structure of the type 37.

When ignoring the  $\tilde{z}$ -component of velocity, it is immediate that

$$\tilde{v}^\sigma c^{-2} \tilde{g}_{\sigma\sigma'} \tilde{v}^{\sigma'} \leq 1. \quad (\text{B-8})$$

The relevant geometry is displayed in Figure B-3. We now consider an event from a reflection at a point  $(\tilde{x}_{\text{scat}}, \tilde{y}_{\text{scat}}, \tilde{z}_{\text{scat}})$  that is reached by the source ray at time  $t_s$  and connects to the receiver by the receiver ray taking as initial time  $t'_s$ . Following the propagation of singularities in  $\tilde{D}$ , the “horizontal” sunken source coordinates satisfy

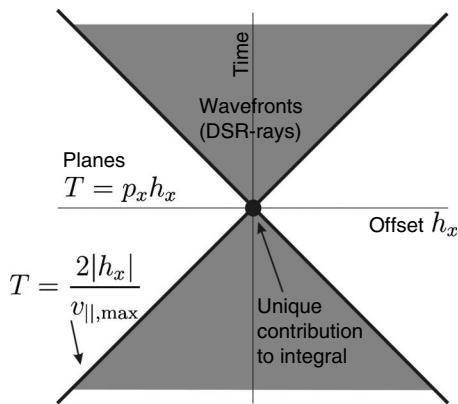


Figure B-2. Cone in phase space for energy admitted to angle-gather construction.

$$\tilde{x}_{\text{scat}} - (\tilde{x} - \tilde{h}_x) = \int_{t'_s}^{t_s} dt \tilde{v}_{s,x}(t), \quad (\text{B-9})$$

$$\tilde{y}_{\text{scat}} - (\tilde{y} - \tilde{h}_y) = \int_{t'_s}^{t_s} dt \tilde{v}_{s,y}(t);$$

the “horizontal” sunken receiver coordinates satisfy

$$-\tilde{x}_{\text{scat}} + (\tilde{x} + \tilde{h}_x) = \int_{t'_s}^{t_s} dt \tilde{v}_{r,x}(t), \quad (\text{B-10})$$

$$-\tilde{y}_{\text{scat}} + (\tilde{y} + \tilde{h}_y) = \int_{t'_s}^{t_s} dt \tilde{v}_{r,y}(t).$$

Adding up these equations results in

$$2\tilde{h}_x = \int_{t'_s}^{t''_s} dt \tilde{v}_x(t), \quad 2\tilde{h}_y = \int_{t'_s}^{t''_s} dt \tilde{v}_y(t), \quad (\text{B-11})$$

where  $(\tilde{v}_x(t), \tilde{v}_y(t))$  is taken from the source ray for  $t < t_s$  and from the receiver ray for  $t > t_s$ .

We introduce a tensor  $B_{\sigma\sigma'}$  that is assumed to satisfy the “bound” (cf. equation B-8)

$$w^\sigma B_{\sigma\sigma'} w^{\sigma'} \leq w^\sigma c^{-2} \tilde{g}_{\sigma\sigma'} w^{\sigma'}. \quad (\text{B-12})$$

Using the particular structure of the metric tensor, we obtain the estimate

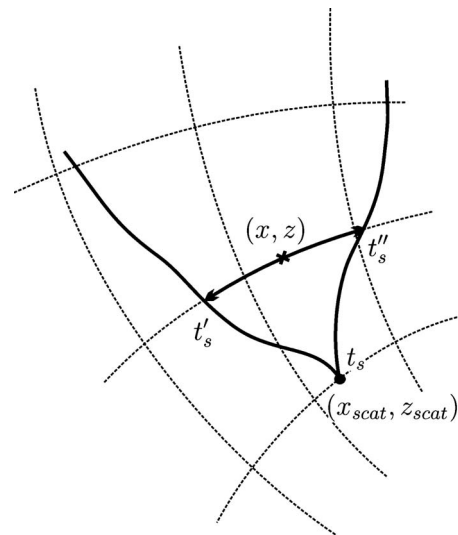


Figure B-3. Ray geometry for offset-time angle-gather construction with respect to curvilinear coordinates.

$$2(\tilde{h}^\sigma B_{\sigma\sigma'} \tilde{h}^{\sigma'})^{1/2} \leq \int_{t'_s}^{t''_s} (\tilde{v}^\sigma c^{-2} \tilde{g}_{\sigma\sigma'} \tilde{v}^{\sigma'})^{1/2} dt \leq |t'_s - t''_s| = |T|, \quad (\text{B-13})$$

which replaces equation B-4. We conclude that the energy in  $\tilde{D}$  is located within the cone in  $(\tilde{h}_x, \tilde{h}_y, T)$  space defined by this equation.

The angle transform is an integral of  $\tilde{D}$  over a plane in  $(\tilde{h}_x, \tilde{h}_y, T)$  space given by  $T = \tilde{p}_\sigma \tilde{h}^\sigma$ . Let  $B^{\sigma\sigma'}$  denote the elements of the inverse of the matrix  $B_{\sigma\sigma'}$ . Suppose that

$$\tilde{p}_\sigma B^{\sigma\sigma'} \tilde{p}_{\sigma'} < 2, \quad (\text{B-14})$$

which replaces equation B-6. With

$$|\tilde{p}_\sigma \tilde{h}^\sigma| \leq (\tilde{p}_\sigma B^{\sigma\sigma'} \tilde{p}_{\sigma'})^{1/2} (\tilde{h}^\sigma B_{\sigma\sigma'} \tilde{h}^{\sigma'})^{1/2}, \quad (\text{B-15})$$

it then follows that

$$|T| = |\tilde{p}_\sigma \tilde{h}^\sigma| < 2(\tilde{h}^\sigma B_{\sigma\sigma'} \tilde{h}^{\sigma'})^{1/2}, \quad (\text{B-16})$$

which replaces equation B-7. Using the same arguments as before, it follows, again, that the energy in the angle transform (cf. equation 48) is located only at the true scattering point independent of  $\tilde{p}$ .

## REFERENCES

- Albertin, U., P. C. Sava, J. Etgen, and M. Maharramov, 2006, Adjoint wave-equation velocity analysis: 76th Annual International Meeting, SEG, Expanded Abstracts, 3345–3348.
- Albertin, U., D. Watts, W. Chang, S. J. Kapoor, C. Stork, P. Kitchenside, and D. Yingst, 2002, Near-salt-flank imaging with Kirchhoff and wavefield-extrapolation migration: 72nd Annual International Meeting, SEG, Expanded Abstracts, 1328–1331.
- Barley, B., and T. Summers, 2007, Multi-azimuth and wide-azimuth seismic: Shallow to deep water, exploration to production: The Leading Edge, **26**, 450–457.
- Biondi, B., 2003, Equivalence of source-receiver migration and shot-profile migration: Geophysics, **68**, 1340–1347.
- Biondi, B., and G. Shan, 2002, Prestack imaging of overturned reflections by reverse time migration: 72nd Annual International Meeting, SEG, Expanded Abstracts, 1284–1287.
- Biondi, B., and W. W. Symes, 2004, Angle-domain common-image gathers for migration velocity analysis by wavefield-continuation imaging: Geophysics, **69**, 1283–1298.
- Brandsberg-Dahl, S., M. V. de Hoop, and B. Ursin, 2003, Focusing in dip and AVA compensation on scattering angle/azimuth common image gathers: Geophysics, **68**, 232–254.
- Claerbout, J. F., 1971, Toward a unified theory of reflector mapping: Geophysics, **36**, 467–481.
- , 1985, Imaging the earth's interior: Blackwell Scientific Publishers.
- De Bruin, C. G. M., C. P. A. Wapenaar, and A. J. Berkhout, 1990, Angle-dependent reflectivity by means of prestack migration: Geophysics, **55**, 1223–1234.
- De Hoop, M. V., 2004, The downward continuation approach to modeling and inverse scattering of seismic data in the Kirchhoff approximation: Contemporary Mathematics, **362**, 211–232.
- De Hoop, M. V., and N. Bleistein, 1997, Generalized Radon transform inversions for reflectivity in anisotropic elastic media: Inverse Problems, **13**, 669–690.
- De Hoop, M. V., J. Le Rousseau, and B. Biondi, 2003, Symplectic structure of wave-equation imaging: A path-integral approach based on the double-square-root equation: Geophysical Journal International, **153**, 52–74.
- De Hoop, M. V., R. D. Van der Hilst, and P. Shen, 2006, Wave-equation reflection tomography: Annihilators and sensitivity kernels: Geophysical Journal International, **167**, 1332–1352.
- Duistermaat, J. J., 1973, Fourier integral operators: Lecture notes: Courant Institute of Mathematical Sciences, New York University.
- Faye, J. P., and J. P. Jeannot, 1986, Prestack migration velocities from focusing depth analysis: 56th Annual International Meeting, SEG, Expanded Abstracts, 438–440.
- Fliedner, M. M., S. Crawley, D. Bevc, A. M. Popovici, and B. Biondi, 2002, Imaging of a rugose salt body in the deep Gulf of Mexico: Kirchhoff versus common azimuth wave-equation migration: 72nd Annual International Meeting, SEG, Expanded Abstracts, 1304–1307.
- Fomel, S., 2004, Theory of 3-D angle gathers in wave-equation imaging: 74th Annual International Meeting, SEG, Expanded Abstracts, 1053–1056.
- Friedlander, F. G., 1976, The wave equation on a curved space-time: Cambridge University Press.
- Hörmander, L., 1983, The analysis of linear partial differential operators, vol. 1: Springer-Verlag.
- Joncour, F., G. Lambaré, J. Svay-Lucas, and B. Duquet, 2005, True amplitude migration by wavefield continuation: 75th Annual International Meeting, SEG, Expanded Abstracts, 1942–1945.
- Kleyn, A., 1983, Seismic reflection interpretation: Applied Science Publishers.
- MacKay, S., and R. Abma, 1992, Imaging and velocity estimation with depth-focusing analysis: Geophysics, **57**, 1608–1622.
- Michell, S., E. Shoshitaishvili, D. Chergotis, J. Sharp, and J. Etgen, 2006, Wide azimuth streamer imaging of Mad Dog: Have we solved the subsalt imaging problem?: 76th Annual International Meeting, SEG, Expanded Abstracts, 2905–2909.
- Nemeth, T., 1995, Velocity estimation using tomographic depth-focusing analysis: 65th Annual International Meeting, SEG, Expanded Abstracts, 465–468.
- Nolan, C. J., and W. W. Symes, 1996, Imaging and coherency in complex structure: 66th Annual International Meeting, SEG, Expanded Abstracts, 359–363.
- , 1997, Global solution of a linearized inverse problem for the wave equation: Communications in Partial Differential Equations, **22**, 919–952.
- Prucha, M., B. Biondi, and W. W. Symes, 1999, Angle-domain common image gathers by wave-equation migration: 69th Annual International Meeting, SEG, Expanded Abstracts, 824–827.
- Rakesh, 1988, A linearized inverse problem for the wave equation: Communications in Partial Differential Equations, **13**, 573–601.
- Sava, P., and B. Biondi, 2004, Wave-equation migration velocity analysis: 1 — Theory: Geophysical Prospecting, **52**, 593–606.
- Sava, P., and S. Fomel, 2003, Angle-domain common-image gathers by wavefield continuation methods: Geophysics, **68**, 1065–1074.
- , 2005a, Coordinate-independent angle-gathers for wave equation migration: 75th Annual International Meeting, SEG, Expanded Abstracts, 2052–2055.
- , 2005b, Riemannian wavefield extrapolation: Geophysics, **70**, no. 3, T45–T56.
- Schultz, P., and J. Sherwood, 1982, Depth migration before stack: Geophysics, **45**, 376–393.
- Shen, P., W. W. Symes, and C. C. Stolk, 2003, Differential semblance velocity analysis by wave-equation migration: 73rd Annual International Meeting, SEG, Expanded Abstracts, 2135–2139.
- Sirgue, L., and R. G. Pratt, 2004, Efficient waveform inversion and imaging: A strategy for selecting temporal frequencies: Geophysics, **69**, 231–248.
- Stolk, C. C., 2002, Microlocal analysis of the scattering angle transform: Communications in Partial Differential Equations, **27**, 1879–1900.
- Stolk, C. C., and M. V. de Hoop, 2001, Seismic inverse scattering in the “wave-equation” approach: The Mathematical Sciences Research Institute, Berkeley, Preprint 2001-047, accessed 15 December 2001: <http://msri.org/publications/preprints/2001.html>.
- , 2005, Modeling of seismic data in the downward continuation approach: SIAM Journal on Applied Mathematics, **65**, 1388–1406.
- , 2006, Seismic inverse scattering in the downward continuation approach: Wave Motion, **43**, 579–598.
- Stolk, C. C., and W. W. Symes, 2004, Kinematic artifacts in prestack depth migration: Geophysics, **69**, 562–575.
- Taylor, M., 1981, Pseudodifferential operators: Princeton University Press.
- Xu, S., H. Chauris, G. Lambaré, and M. Noble, 2001, Common angle migration: A strategy for imaging complex media: Geophysics, **66**, 1877–1894.

Yilmaz, O., 1987, Seismic data processing: SEG Investigations in Geophysics No. 2.

Yoon, K., C. Shin, S. Suh, L. Lines, and S. Hong, 2003, 3D reverse-time migration using the acoustic wave equation: An experience with the SEG/

EAGE data set: The Leading Edge, **22**, 38–41.

Zhang, Y., S. Xu, N. Bleistein, and G. Zhang, 2007, True-amplitude, angle-domain, common-image gathers from one-way wave-equation migration: Geophysics, **72**, no. 1, S49–S58.